February 2000 • NREL/SR-520-27931

Subcontractor Report

Photocharge Transport and Recombination Measurements in Amorphous Silicon Films and Solar Cells by Photoconductive Frequency Mixing

Annual Subcontract Report
20 April 1998 — 19 April 1999

R. Braunstein, A. Kattwinkel, J. Liebe, and G. Sun
Department of Physics and Astronomy
University of California
Los Angeles, California

National Renewable Energy Laboratory

1617 Cole Boulevard
Golden, Colorado 80401-3393

NREL is a U.S. Department of Energy Laboratory
Operated by Midwest Research Institute • Battelle • Bechtel

Contract No. DE-AC36-99-GO10337

February 2000 • NREL/SR-520-27931

Photocharge Transport and Recombination Measurements in Amorphous Silicon Films and Solar Cells by Photoconductive Frequency Mixing

Annual Subcontract Report
20 April 1998 — 19 April 1999

R. Braunstein, A. Kattwinkel, J. Liebe, and G. Sun
Department of Physics and Astronomy
University of California
Los Angeles, California

NREL Technical Monitor: B. Von Roedern

Prepared under Subcontract No. XAK-8-17619-24

National Renewable Energy Laboratory

1617 Cole Boulevard
Golden, Colorado 80401-3393

NREL is a U.S. Department of Energy Laboratory
Operated by Midwest Research Institute • Battelle • Bechtel

Contract No. DE-AC36-99-GO10337

NOTICE

Available electronically at http://www.doe.gov/bridge

Available for a processing fee to U.S. Department of Energy
and its contractors, in paper, from:

U.S. Department of Energy
Office of Scientific and Technical Information
P.O. Box 62
Oak Ridge, TN 37831-0062
phone: 865.576.8401
fax: 865.576.5728
email: reports@adonis.osti.gov

Available for sale to the public, in paper, from:

U.S. Department of Commerce
National Technical Information Service
5285 Port Royal Road
Springfield, VA 22161
phone: 800.553.6847
fax: 703.605.6900
email: orders@ntis.fedworld.gov
online ordering: http://www.ntis.gov/ordering.htm

Printed on paper containing at least 50% wastepaper, including 20% postconsumer waste

Preface

The National Amorphous Silicon research team consists of focused subteams to improve the individual component cells from which the multijunction devices are fabricated. The Mid-bandgap and Metastability subteam and the Low Bandgap subteam have the responsibility to develop appropriate materials for the respective layer of the triple junction solar cell. To this end, it is necessary to characterize the materials that are prepared for the appropriate layer to optimize the devices and to develop an understand of the conditions responsible for light-induced degradation so as to develop means to mitigate the degradation. Using the photomixing technique, UCLA was able to determine the mobility and lifetime separately of a number of semiconductor materials. We have established that different kinetics of degradation occur for mobility and lifetime. We have found that the drift mobility is electric field dependent and developed a model for the charge transport through long range potential fluctuations which enable a determination of the range and the depth of these fluctuations for material in the annealed and light soaked states. UCLA has continued to provide transport parameters for the mid-gap, metastability, and low- band teams. The materials studied were prepared by various deposition techniques.

In phase I of this program, we have determined the transport parameters by photomixing of materials prepared by the hot wire chemical vapor deposition technique. This has included a-Si:H, μc Si:H and SiGe:H alloys films. Photomixing experiments were initiated on p-i-n devices. Measurements of the transport parameters under hydrostatic pressure were initiated to investigated whether the application of hydrostatic pressure can alter light induced degradation behavior and as a possible test of the various theories that have been recently been developed to explain the cause of light-degradation involving the mobility of hydrogen.

Table of Contents

List of Figures

List of Tables

Introduction

In the present phase of the program, the transport parameters of a number of amorphous semiconductors prepared by a number of techniques were determined by the photoconductive frequency mixing technique. This technique enabled us to determine the drift mobility, μ_d, and the photomixing lifetime, τ. The technique is based on the idea of heterodyne detection for photoconductors. When two similarly polarized monochromatic optical beams of slightly different frequencies are incident upon a photoconductor, the generation rate of electron-hole pairs will produce a photocurrent, when a dc- bias is applied, which will contain components resulting from the square of the sum of the individual incident fields. Consequently, a photocurrent will be produced, which will consist of a dc- and a microwave current corresponding to the beat frequency. These two currents allow a separate determination of the drift mobility and the photomixing lifetime of the photogenerated carriers [1-6]. In the present work, the longitudinal modes of a He-Ne laser were employed to generate a beat frequency of 252 MHz; all the measurements were performed at this frequency for the data indicated in the accompanying figures. Employing this technique, the following topics were explored whose results will be presented in the following sections:

1. Measurements of the charge transport parameters of homogeneous a-SiGe:H alloys produced by NREL employing the hot-wire technique.
2. The change in the charge transport parameters in the transition from hydrogenated amorphous silicon to microcrystalline silicon for material produced by NREL and MVSystems.
3. The improvement in instrumentation of the photomixing measurements.
4. Measurements of the hydrostatic dependency of the transport parameters of amorphous silicon
5. Preliminary measurements on p-i-n devices.

1. Measurements of homogenous SiGe alloy samples produced at NREL

The a-SiGe:H sub-team at NREL is presently employing the hot-wire technique to produce a-SiGe:H alloys which are to be optimized with respect to the transport parameters within two bandgap regimes: 1.40-1.45 eV to 1.60-1.65 eV. We have previously determined the transport parameters of a series a-SiGe:H alloys supplied by Brent Nelson where he explored the parameter space involving the number of collisions a reactive species makes before impinging on the substrate surface. These measurements involved a range of preparation parameters which resulted in inhomogeneity of composition. We now report on a series of samples that are homogeneous in alloy composition supplied by Nelson. The photoconductivity, drift mobility, and lifetime were studied systematically in the annealed and light-soaked states employing the photomixing technique using the longitudinal modes of a HeNe laser. All the samples were initially annealed at 150^0C for 2 hours to restore the samples to the annealed state. The characteristics of the samples are listed in Table 1.

Table 1. *The characteristics of a-SiGe:H and a-Si:H.*

Sample ID	Substrate Temp. ^{0}C	GeH_4 (%)	Thickness (μm)
HGe118	400	0	1.093
HGe114	475	3	1.447
HGe121	365	3	1.858
HGe113	475	8	1.482
HGe100	500	17	2.055

Figure 1 shows the normalized photoconductivity, mobility, and lifetime for a-Si:H prepared by the same hot-wire technique as a function of illumination time. During illumination, both the drift mobility and lifetime decrease. This is consistent with previous results we have obtained indicating that both neutral and charged defects are created by light-soaking.

Figures 2-5 show the normalized photoconductivity, mobility, and lifetime in a-SiGe:H alloys prepared with different GeH_4 gas flow ratios as a function of illumination time. It can be seen from these results that both the mobility and lifetime are lowered by light-soaking which is similar to a-Si:H; however it should be noted that the rate of decrease of these quantities varies as a function of the sample composition. We have also measured the electric field dependence of the mobility and thus determined the range and the depth of the long-range potential fluctuations. The results for the annealed state are shown in Table 2 while the results for the light-soaked state are shown in Table 3.

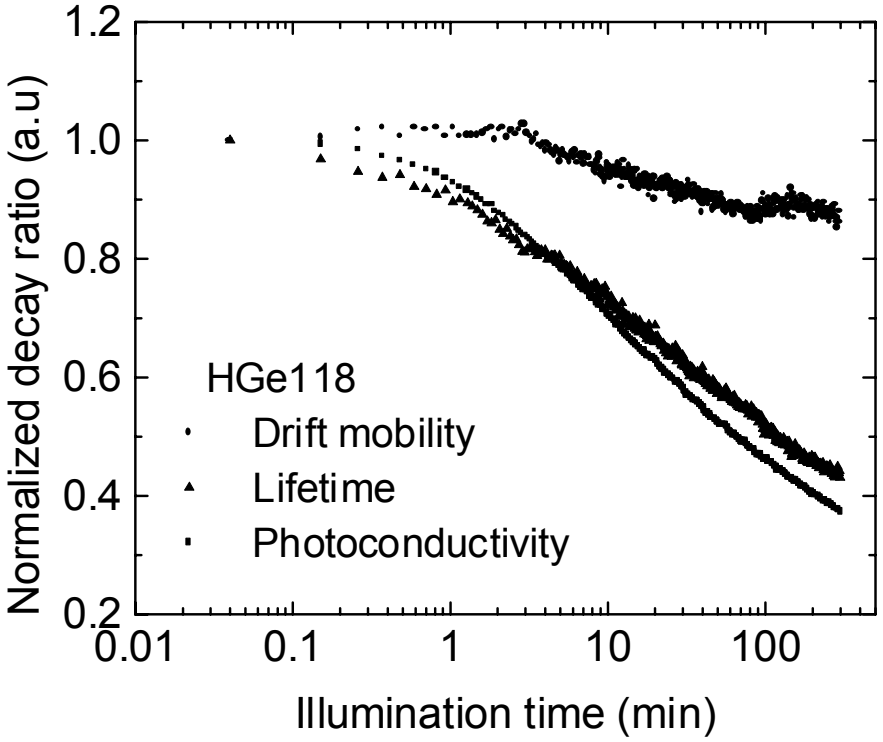

Figure 1. *The normalized photoconductivity, mobility, and lifetime in a-Si:H as a function of illumination time.*

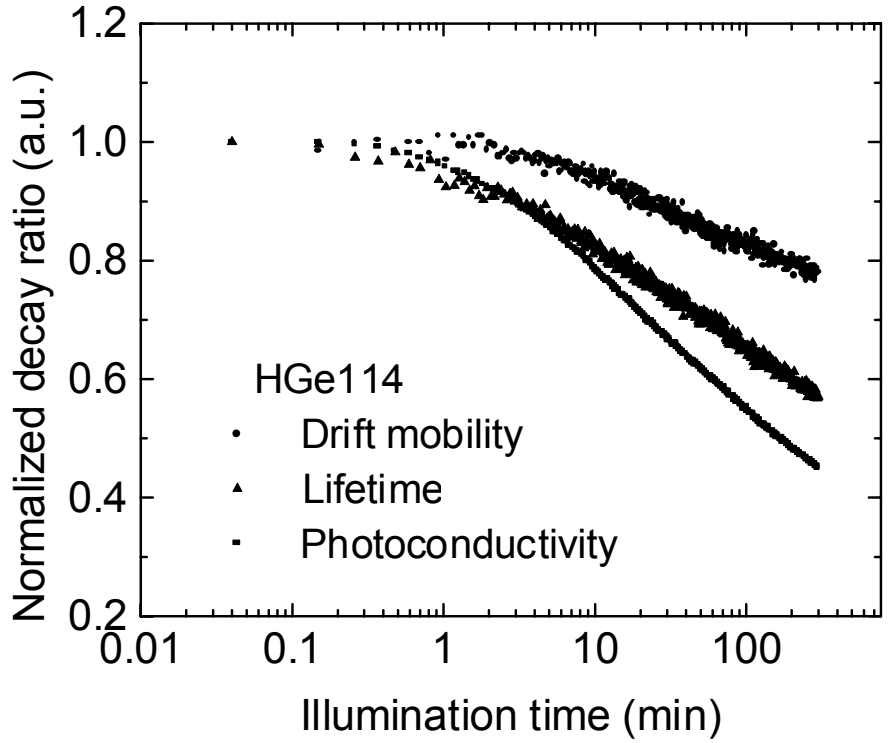

Figure 2. *The normalized photoconductivity, mobility, and lifetime as a function of illumination time. The GeH_4 gas flow ratio is 3%.*

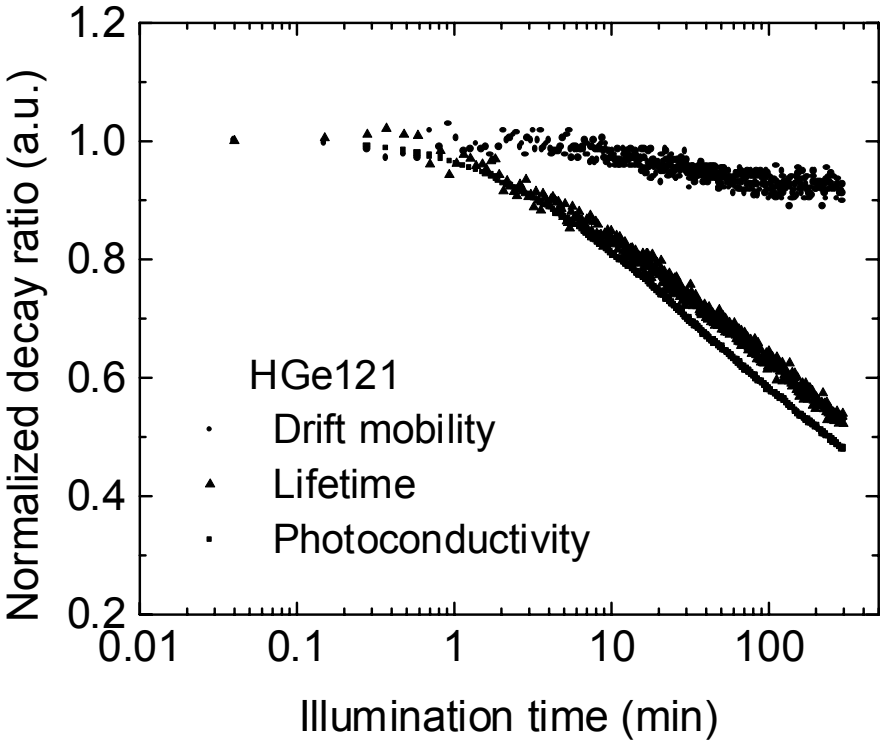

Figure 3. *The normalized photoconductivity, mobility, and lifetime as a function of illumination time. The GeH_4 gas flow ratio is 3%.*

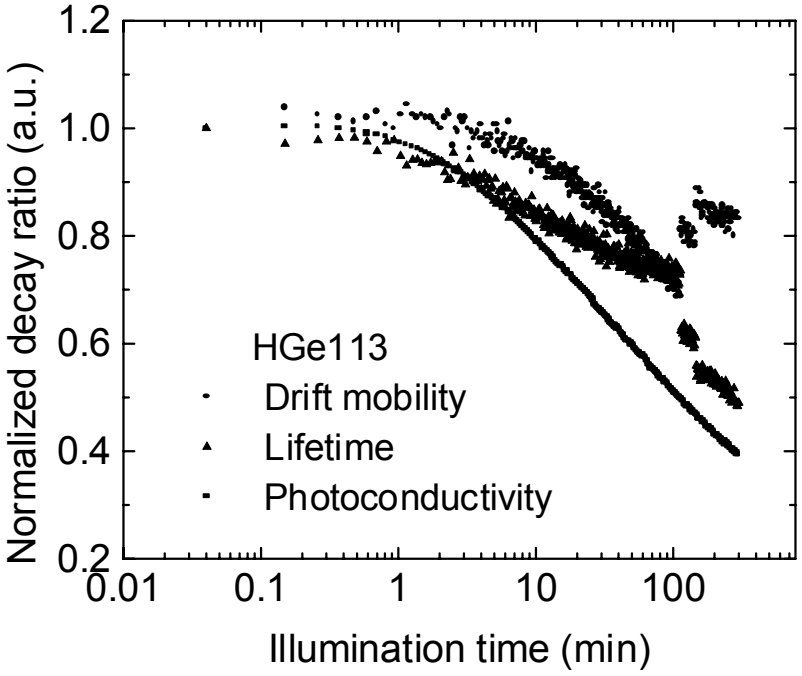

Figure 4. *The normalized photoconductivity, mobility, and lifetime as a function of illumination time. The GeH_4 gas flow ratio is 8%.*

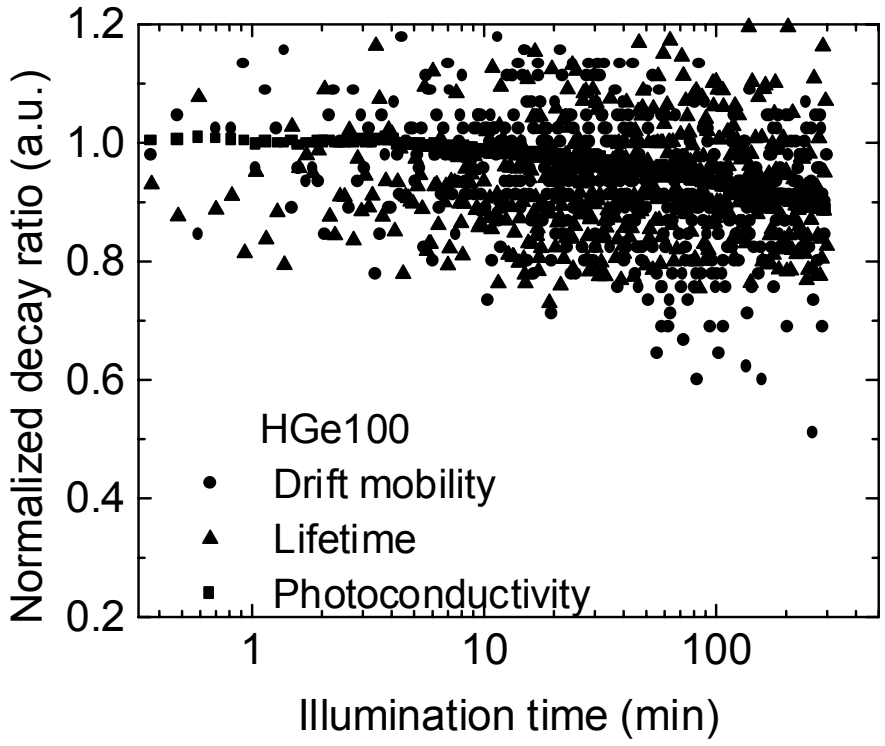

Figure 5. *The normalized photoconductivity, mobility, and lifetime as a function of illumination time. The GeH_4 gas flow ratio is 17%.*

Table 2. *The photoconductivity, drift mobility, lifetime, and range and depth of long range potential fluctuations in **annealed** state for a-SiGe:H alloys prepared with different GeH_4 gas flow ratio.*

	HGe100	HGe113	HGe121	HGe114	HGe118
GeH_4	17%	8%	3%	3%	0%
σ_{ph} ($\Omega^{-1}cm^{-1}$)	0.31×10^{-4}	3.72×10^{-4}	1.39×10^{-4}	3.40×10^{-4}	5.91×10^{-4}
τ (ns)	49.87	179.00	62.42	86.00	71.28
μ_d (cm^2/Vs)	0.067	0.160	0.216	0.303	0.473
L (nm)	25.61	34.46	29.05	38.24	41.24
V_p (eV)	0.143	0.117	0.109	0.103	0.092

Table 3. *The photoconductivity, drift mobility, lifetime, and range and depth of long range potential fluctuations in **light-soaked** state for a-SiGe:H alloys prepared with different GeH_4 gas flow ratio.*

	HGe100	HGe113	HGe121	HGe114	HGe118
GeH_4	17%	8%	3%	3%	0%
σ_{ph} ($\Omega^{-1}cm^{-1}$)	0.27×10^{-4}	1.46×10^{-4}	0.67×10^{-4}	1.53×10^{-4}	2.21×10^{-4}
τ (ns)	41.96	87.72	32.60	49.33	30.67
μ_d (cm^2/Vs)	0.065	0.133	0.194	0.242	0.425
L (nm)	57.40	29.00	20.62	21.29	26.79
V_p (eV)	0.158	0.123	0.109	0.104	0.093

In the annealed state, the photoconductivity, drift mobility, lifetime and the range of the long-range potential fluctuations in a-SiGe:H decrease, while the depth of the long-range potential fluctuations increases with increasing GeH_4 gas flow ratio. The number of charge states can be estimated using the range and depth of the long-range potential fluctuations due to charge states; some of the charge states can be due to the effect of alloying whereby the neutral homopolar bonds of Ge-Ge and Si-Si get modified in the case of a Ge-Si bonds resulting in a slight ionic character.

The surface morphology of these samples were determined by AFM in cooperation with Dr. David Braunstein formerly of Parks Scientific and presently of IBM. Figure 6 shows the RMS surface roughness vs. the GeH_4 gas flow rate. The transport parameters as a function of the GeH_4 gas flow rate are shown in Figure 7. Figures 8-12 show the images of the surface scans and the respective surface roughnesses. The surface roughness should not be interpreted as grain size. To arrive at the grain size it is necessary to perform a Fourier analysis of the image which will be reported a later date.

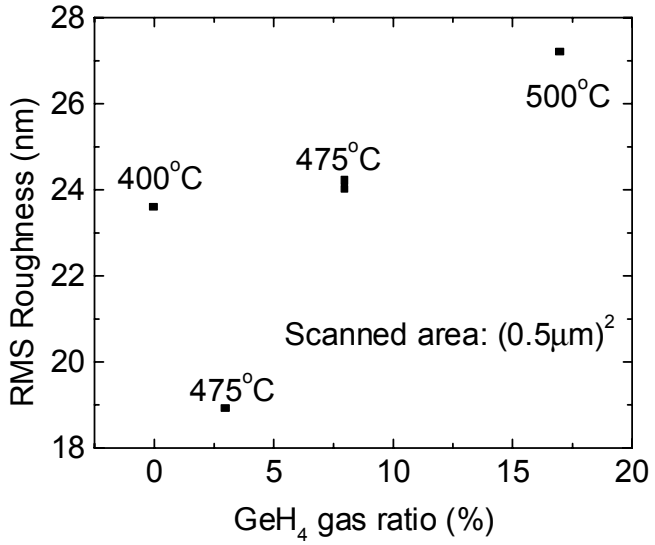

Figure 6: *RMS roughness vs. GeH_4 gas ratio.*

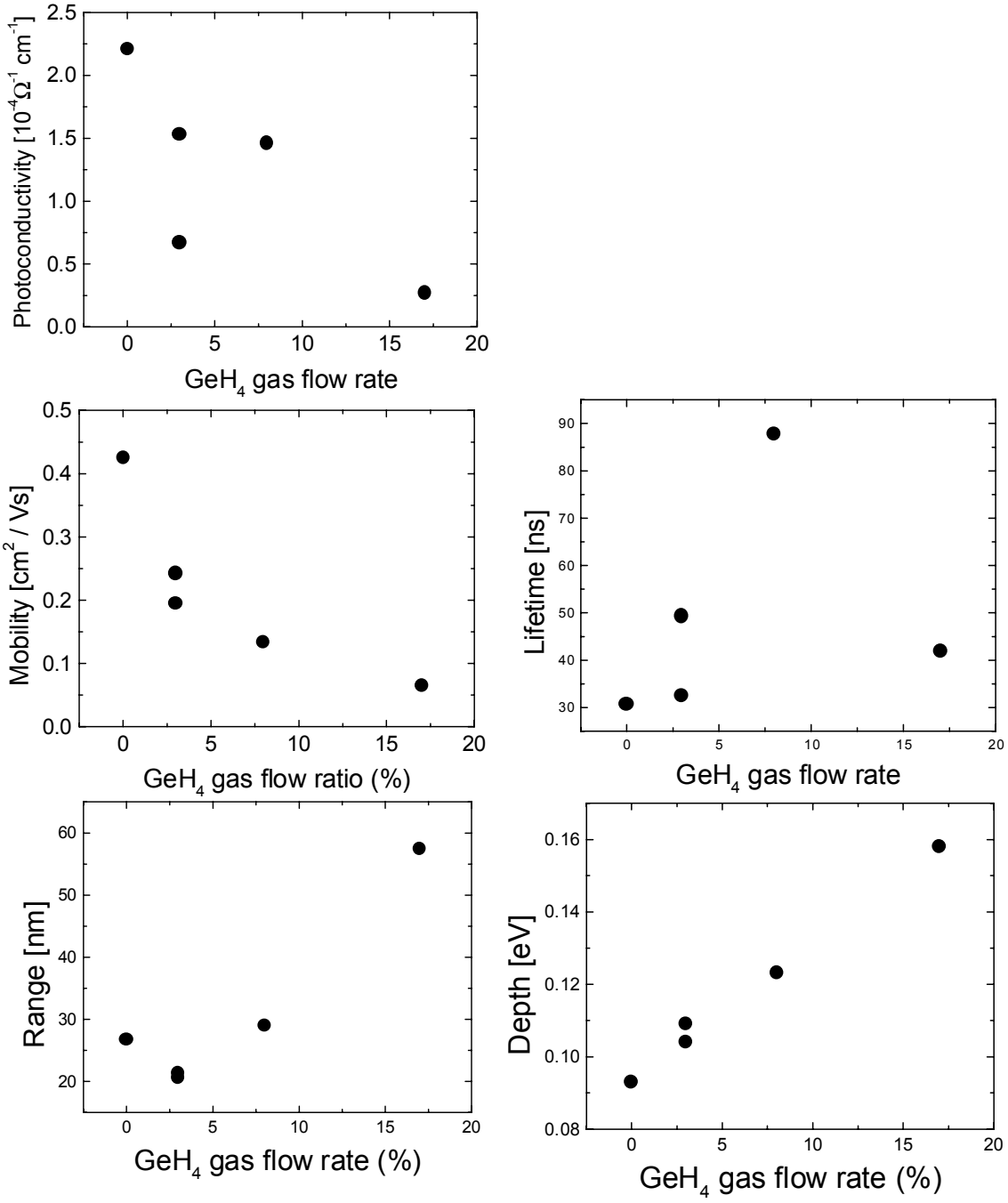

Figure 7: *Photoconductivity, mobility, lifetime, LRPF range and depth vs. germanium hydrogen gas flow ratio (annealed state).*

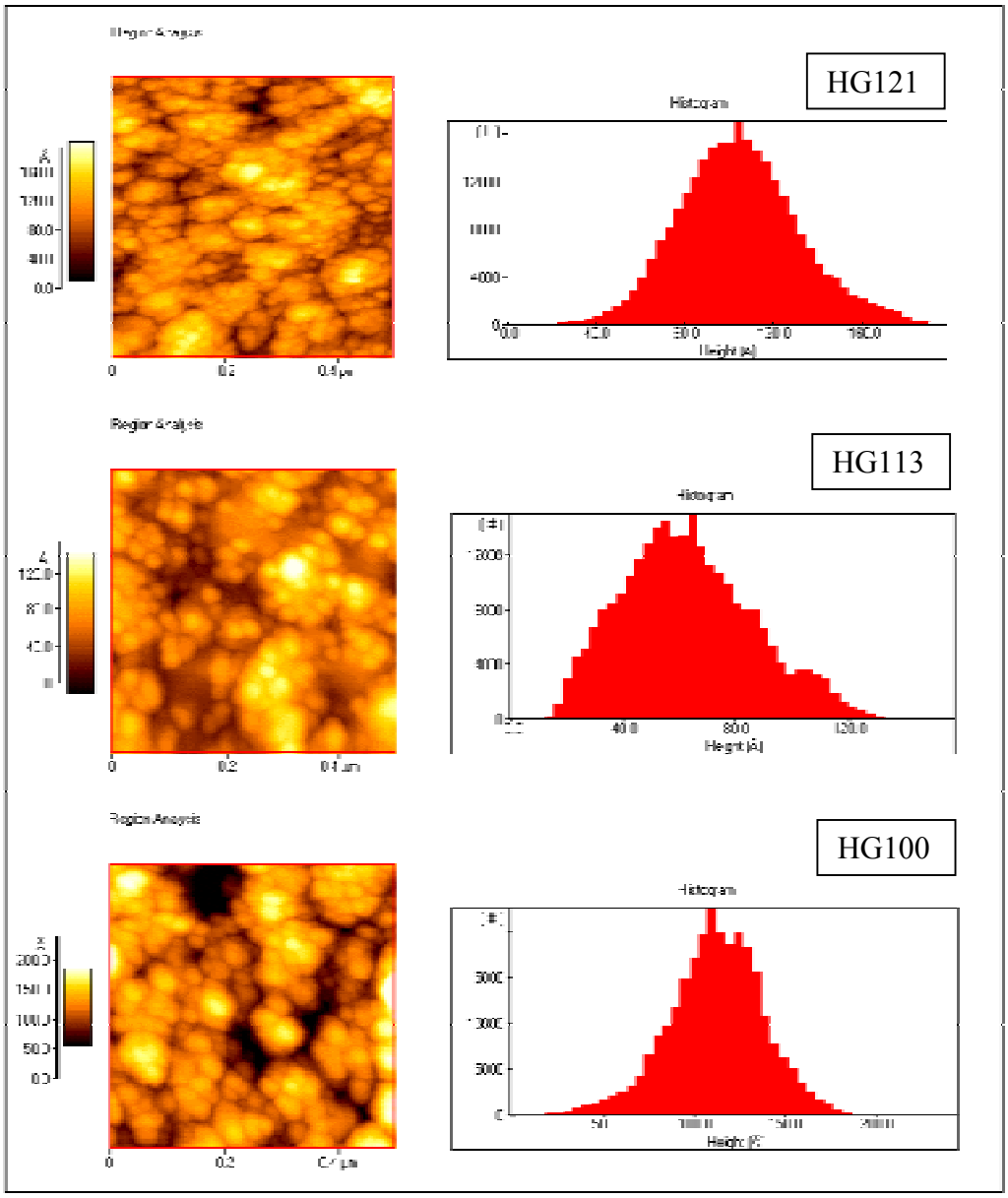

Figures 8-10. *The AFM scanning images and surface height distribution of the samples HGe 121, 113, and 100.*

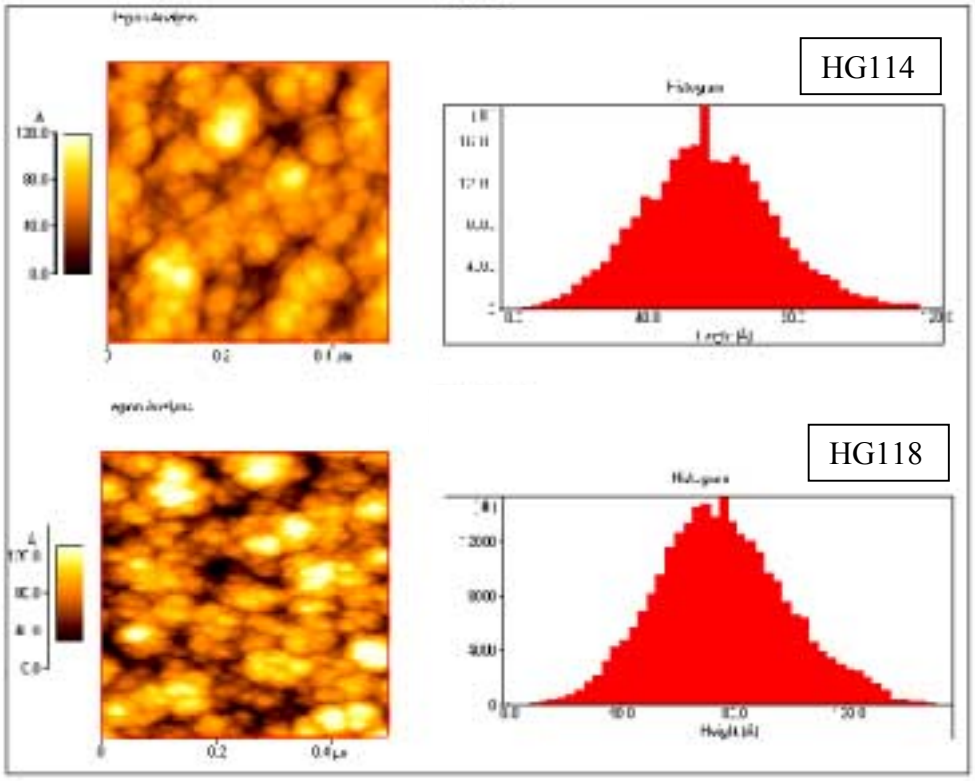

Figures11-12: *The AFM scanning images and surface height distribution of the samples HGe 114 and HGe 118.*

2. Charge transport in the transition from hydrogenated amorphous silicon to microcrystalline silicon

(a) Material produced at NREL

Microcrystalline silicon ($\mu c - Si:H$) has been the object of studies for many years to understand its electronic, optical and structural properties. However, recently there has been a renewed interest in incorporating $\mu c - Si:H$ in different solar cell structures since such devices have shown no degradation after prolonged light soaking [7,8]. It has been shown that a-Si:H films grown under hydrogen dilution close to the onset of microcrystallinity exhibit a higher degree of stability against light soaking compared to a-Si:H. In hot-wire assisted chemical vapor deposition (HW-CVD) [9-13], the decomposition of silane and hydrogen gas mixture allows one to prepare material with a transition from to amorphous to microcrystalline growth by variation of the silane to hydrogen dilution. By varying the grain size, an enhanced absorption of microcrystalline compared to crystalline silicon has been observed [14]. The (HW-CVD) method allows a continuous preparation of material with a smooth transition from amorphous hydrogenated silicon to microsrystalline silicon.The photoconductivity in microcrystalline silicon has been studied as a function of Fermi-level to determine the mobility-lifetime product ($\mu\tau$) [15] with the observation that ($\mu\tau$) increased significantly by shifting the Fermi level from the mid-gap towards the conduction or valence band; this was attributed to the increase in the majority carrier lifetime due to a change in the thermal occupation of defect centers by the shift of the Fermi level. It is of interest to separately determine the mobility and lifetime in the transition from the amorphous to the microcrystalline state; dc photoconductivity measurements determine the $\mu\tau$ product. The independent determination of μ and τ was accomplished by employing the photoconductive frequency mixing technique [1-6]. By observing the increase in the drift mobility as a function of electric field, the range and the depth of the long-range potential fluctuations [4] as a function of hydrogen content and hence the change in these quantities in the transition from amorphous to microcrystalline states were determined.

In this report we present results from electronic transport measurements of a series of samples prepared employing the hot-wire chemical vapor deposition technique supplied by Qi Wang. Within this series a transition from the amorphous to the microcrystalline state is realized. Since there is evidence that one finds improved stability against light-induced degradation in the mixed state it is interesting to study the (photo-) transport properties and stability with respect to this transition. Table 4 shows a summary of the sample characterization:

Table 4: *Summary of the sample characterization results (Qi Wang).*

Sample ID	**H/SiH$_4$**	XRD **Structure**	**(μc) av. Grain size(n)**	Sample **Thickness**	H-content	Deposition rate
T516	1	a-Si		41,400	13.3	17.25
T517	5	μc Si	12	21,350	5.2	5.93
T518	10	μc Si	13	14,300	4.7	3.97
T519	20	μc Si	14	11,200	3.9	2.33
T528	5	μc Si	18	25,400	3.1	7.05
T529	4	μc Si	12	24,000	4.2	8.00
T530	3	a-Si+μc Si	9	16,400	4.4	7.80
T531	2	a-Si		25,000	8.9	10.41
T532	3	a-Si+μc Si	11	17,000	4.0	7.08
T534	2	a-Si		30,000	10.9	12.50

Results of photomixing measurements

We employed the photoconductive frequency mixing technique to determine the transport properties in terms of the charge carrier (photomixing) lifetime and mobility as well as the over-all photoresponse.

In a-Si:H, the electronic transport depends tightly on the hydrogen content, so the photoconductivity is usually plotted against the amount of H-atoms introduced into the samples. A look at Table 4 indicates that within this series of samples microcrystalline structure results in a low hydrogen content. Therefore, we decided to plot the transport properties against the hydrogen content, including all given samples, as shown in Figure 13.

With the decrease of the H-content the photoconductivity is more or less constant as long as the hydrogen concentration is over about 5% to 6%. However, it shows a sudden increase when the H-concentration drops below 5%, i.e. the microcrystalline regime is entered.

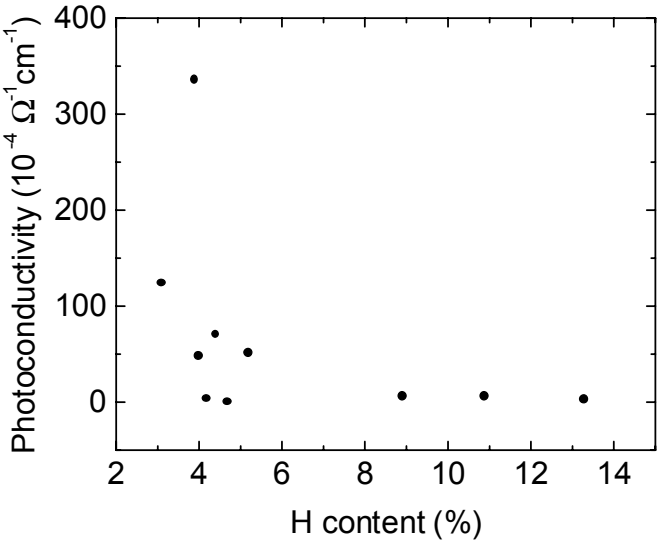

Figure 13: *Photoconductivity of amorphous and microcrystalline silicon vs. hydrogen content.*

To investigate what quantity this increase is due to, we determined the photomixing lifetime τ and mobility μ for each sample in the annealed state. The results are shown in Figures 14 and 15. Both τ and μ are affected by the transition. Similarly to the behavior of the photoconductivity, the lifetime exhibits a sudden increase up to two orders of magnitude when the hydrogen content drops to values less than 5% (Figure 14). The mobility, however, shows somewhat opposite behavior. In the amorphous region, the mobility *increases* with decreasing H-concentration. This is surprising since one usually finds the mobility to increase when the hydrogen content grows. As a comparison, Figure 16 shows the results for a set of samples also produced by hot-wire CVD, but entirely within the amorphous region. For H-contents under 5%, the mobility *drops* to values not detectable anymore. However, except for the samples T518 and T528, μ only drops to about 20% of it's maximum value, so the photoconductivity, being straight proportional to τ and μ, still increases dramatically.

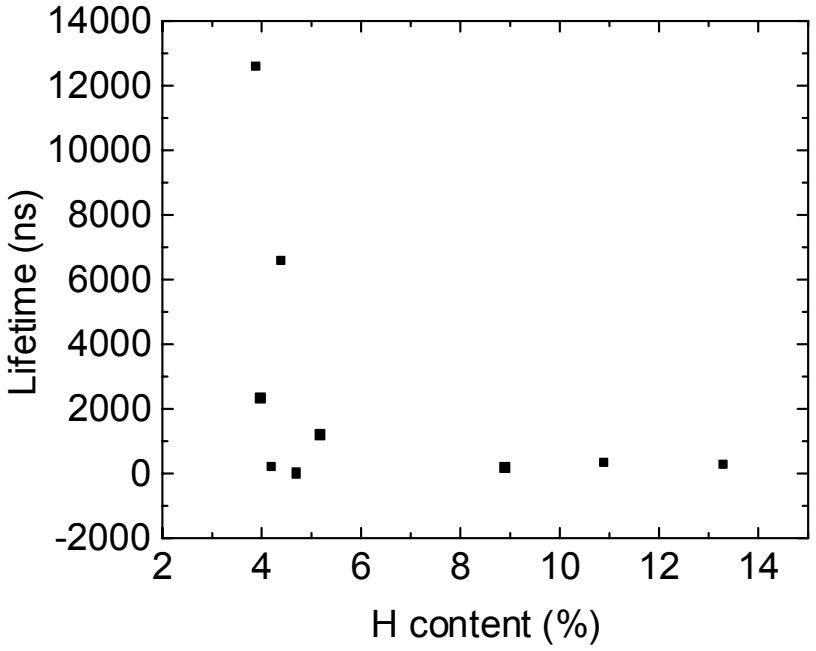

Figure 14: *The photomixing lifetime of amorphous and microcrystalline Si:H vs. hydrogen content.*

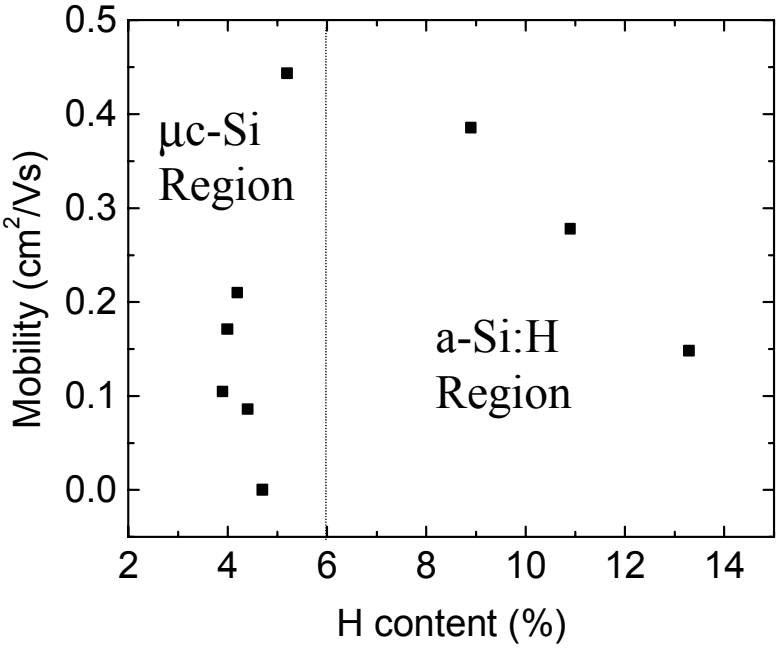

Figure 15: *The mobility of amorphous and microcrystalline Si:H vs. hydrogen content.*

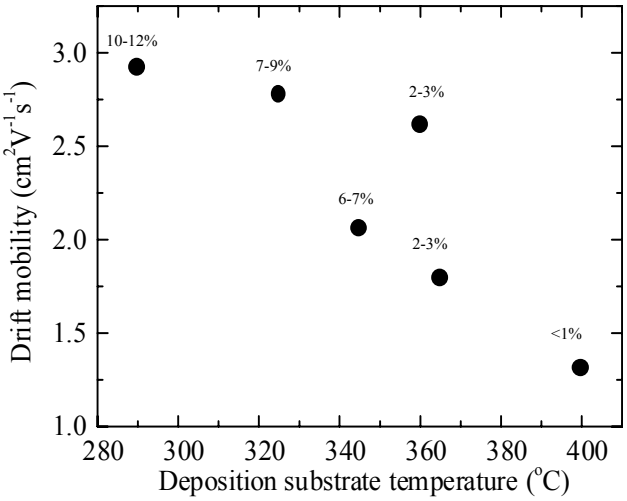

Figure 16: *Drift mobility in the case of entirely amorphous samples (Hot-wire assisted PECVD a-Si:H from NREL).*

Long-Range Potential Fluctuation

Long-range Potential Fluctuations (LRPF) are thought to reflect the density and arrangement of *charged* defects in amorphous silicon. To determine the LRPF within the samples, we performed field-dependent measurements of the mobility and lifetime. The results are shown in Figures 17 and 18. Note that the range increases to values of around 50nm in the μc – regime, which might reflect the occurrence of grain boundaries. Also the depth of the potential fluctuations increases, whereas both quantities decrease with decreasing hydrogen content for H-concentrations over 6% (i.e. the amorphous regime).

These results lead to a possible explanation for both the drop of the mobility and the dramatic increase of the lifetime in the case of microcrystalline silicon. Grain boundaries might serve as scattering centers as well as barriers against recombination.

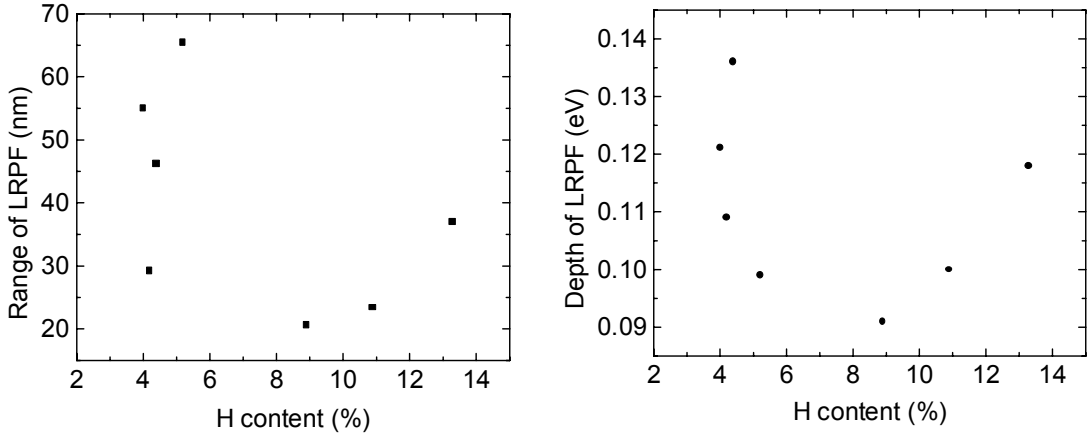

Figures 17 and 18. *Range and depth of long-range potential fluctuations in amorphous and microcrystalline silicon-hydrogen.*

Light-induced Decay Measurements

This section covers measurements of the light-induced degradation (Staebler-Wronski-effect) for samples in the amorphous state, mixed state (a-Si + μc-Si) and the microcrystalline state (μc-Si). Figure 19 shows the normalized photoconductivity for the three amorphous samples, which exhibit behavior as expected from former results. In each case the samples were first annealed for 1 hour at a temperature of 150 ^{0}C.

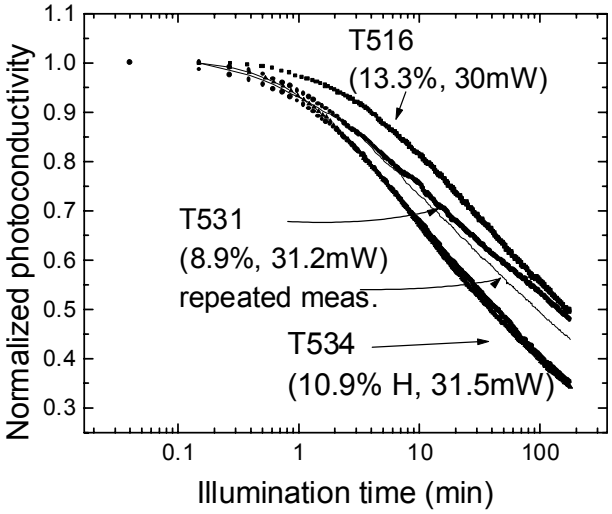

Figure 19. *Normalized photoconductivity vs. illumination duration for T516, T531 and T534 (amorphous state). The light intensities are given in the Figure.*

Since in the case of microcrystalline silicon we found both high dark and photocurrent, we had to restrict the number of points in order to prevent those samples from heating. Also, we could not measure lifetime and mobility at high fields. This results in an increased error and so a certain scattering of both lifetime and mobility. Nonetheless the Figures 20-22 show increased stability against light-induced defects for samples in both the mixed and microcrystalline phase.The increase of the photocurrent in the case of the samples T529 and T532 is probably due to a slight heating.

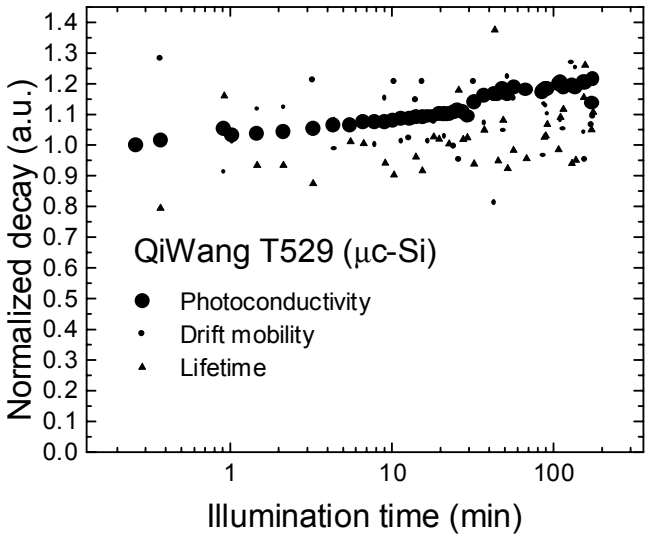

Figure 20. *Photoconductivity, mobility and lifetime vs. illumination duration, T529.*

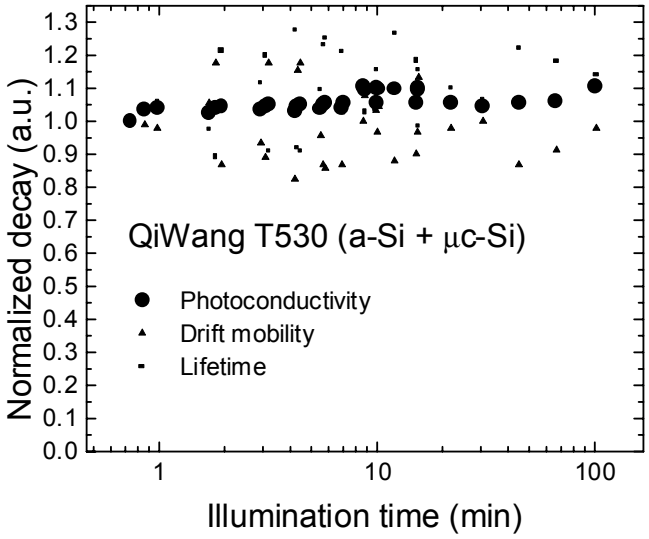

Figure 21. *Photoconductivity, mobility and lifetime vs. illumination duration, T530.*

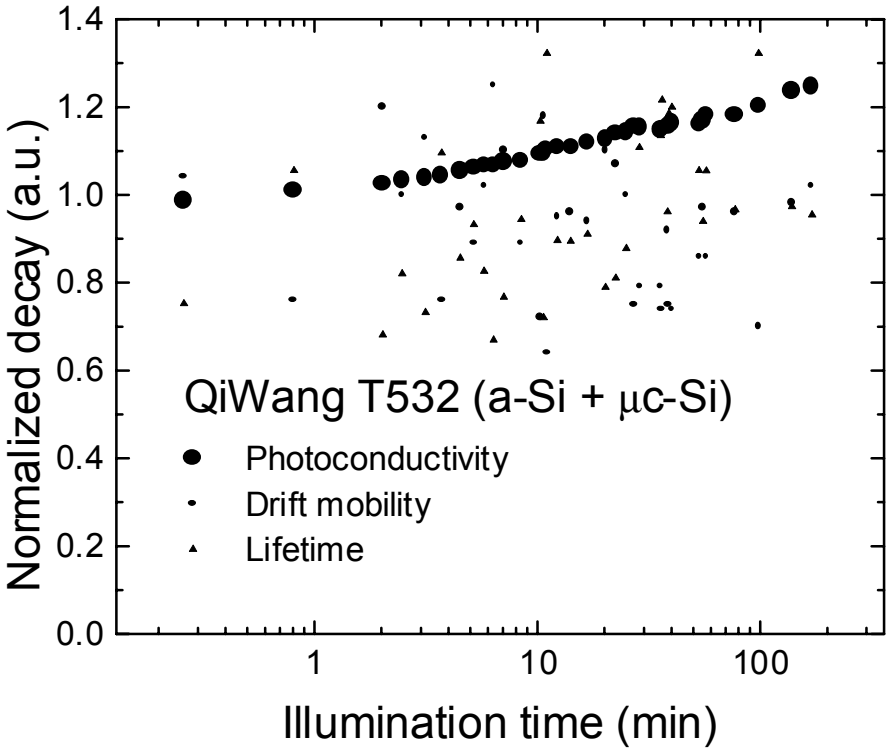

Figure 22. *Photoconductivity, mobility and lifetime vs. illumination duration, T532.*

Summarizing the above results, we found both increased stability and a huge increase of the photomixing lifetime resulting in an increase of the photoresponse for samples entering the microcrystalline regime. The increase in lifetime and decrease in mobility as the microcrystalline regime is entered indicates that grain boundaries can serve as scattering centers as well as barriers against recombination. In order to further illucidate the mechanisms responsible for the dramatic change in lifetime and mobility as one makes the transition from the amorphous to the microcrystalline state, it would be useful to perform similar measurements on samples prepared by different methods which result In different microstructures.

FTIR measurements

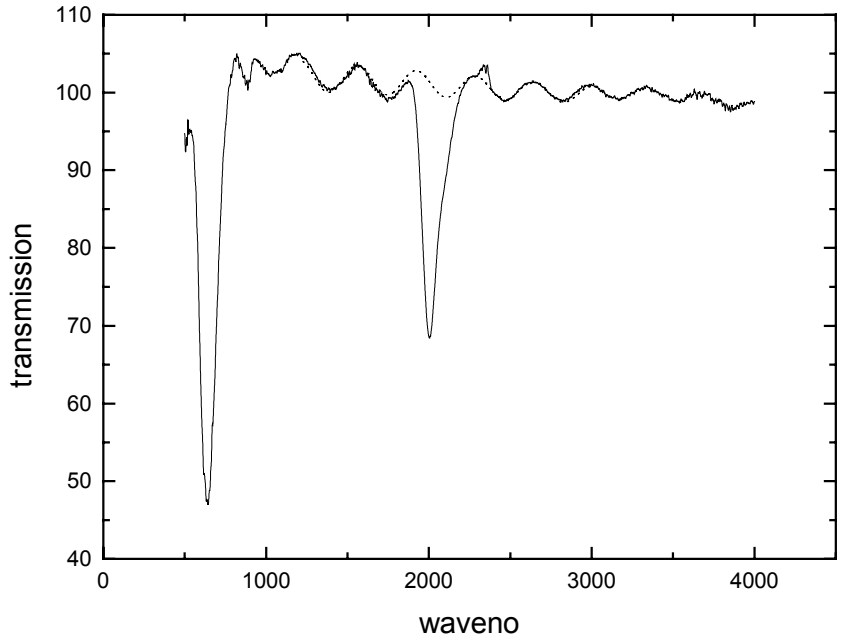

Figure 23. *IR – spectra, sample T516 (a-Si:H) on polycrystalline substrate.*

Figure 23 shows a typical a-Si:H spectrum acquired in the wavelength region from 400 to 4000 cm^{-1}. The total hydrogen content was obtained from the rocking modes of hydrogen in all possible bonding configurations which give rise to an absorption peak at 640cm^{-1}. To calculate the hydrogen content from the integrated absorption of this peak we used values for the oscillation strength parameters given in [16]:

$N_H = AI,$

where N_H is the hydrogen concentration and

$I = \int \frac{\alpha}{\omega} d\omega$

is the integrated absorbance.

and

$$A_{640} = (2.1 \pm 0.2) * 10^{19}\, cm^{-2}$$
$$A_{2000} = (9.0 \pm 1.0) * 10^{19}\, cm^{-2}$$
$$A_{2100} = (2.2 \pm 0.2) * 10^{20}\, cm^{-2}$$

We found good agreement with the values for the hydrogen content given by NREL. The stretching modes at 2000 and 2100cm^{-1} are related to isolated SiH in a Si network or SiH_x, hydrogen clusters, and also SiH bondings at surfaces (e.g. voids) whereas only the latter group gives rise to a 2100 – peak. Figure 24 shows an example of the stretching mode related double-peak in the case of a-Si:H and figure 28 contains the respective deconvolution.

In microcrystalline silicon most hydrogen is bonded at grain boundaries facing intergrain voids and so gives rise to usually at least two peaks around 2100 with respect to the

crystalline grain orientation (figure 25). The intensity ratio of the 2000 and 2100 peaks depends on the dilution as can be seen in figures 25 and 27.

In the mixed state samples, also bending mode related absorption at around 900cm^{-1} occurs as shown in figure 26.

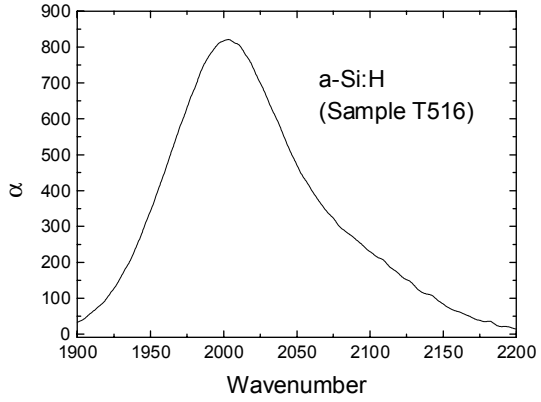

Figure 24. *Stretching modes in a-Si:H. According to this double peak, a significant part of H atoms is bonded as monohydide in a dense Si network.*

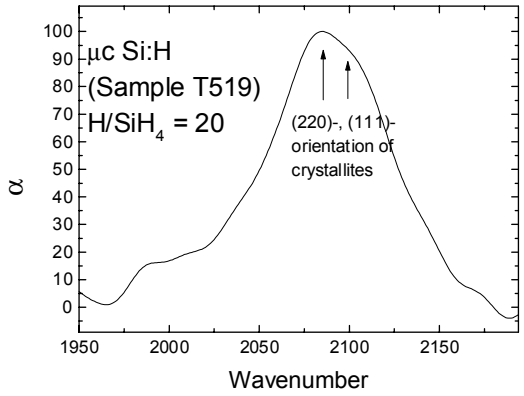

Figure 25. *Stretching modes in microcrystalline silicon – high dilution (note the low 2000 - absorption).*

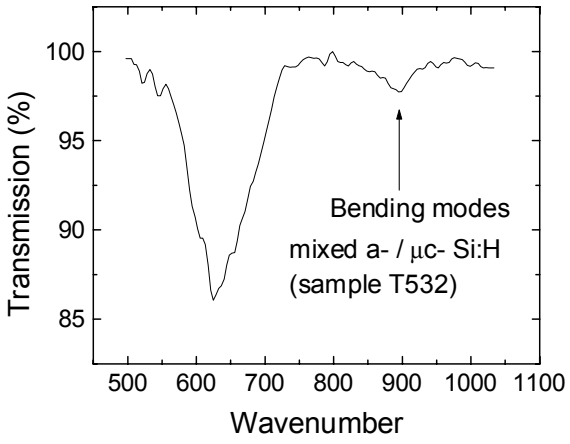

Figure 26. *Bending mode related absorbtion peak at around 900cm^{-1} in the mixed state sample T532.*

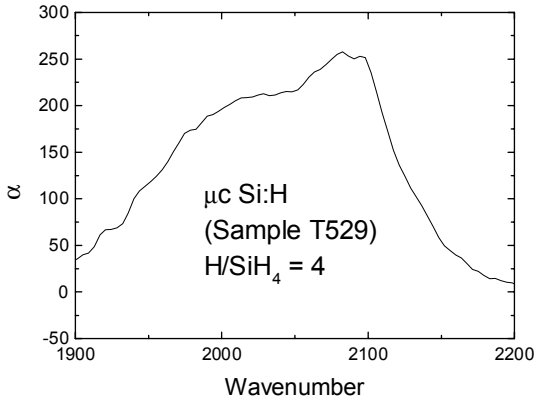

Firgure 27. *Microcrystalline Silicon with low dilution ratio.*

Figure 29 summarizes the stretching modes of samples in the amorphous and mixed state. Note the scaling of the 2000 peak with the dilution ratio.

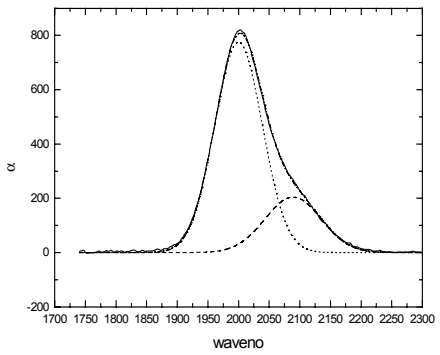

Figure 28.
Deconvolution of 2000/2100-peak (T516).

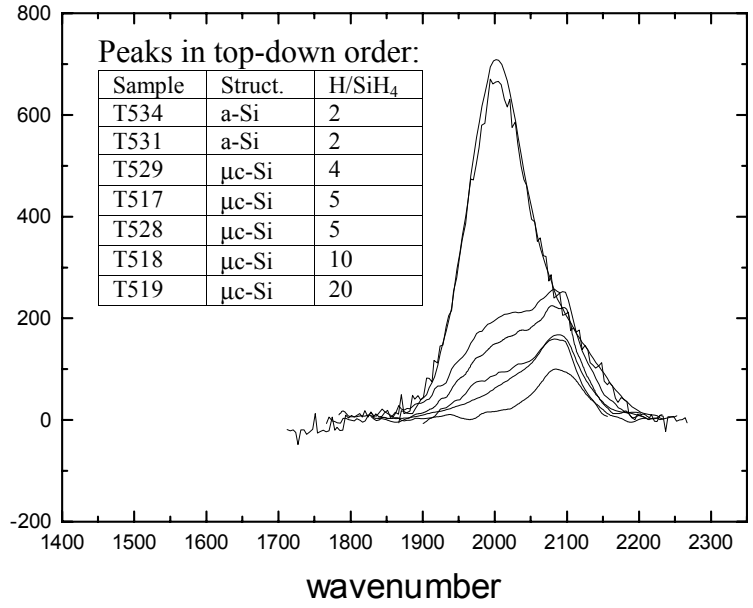

Figure 29. *Stretching modes for several amorphous and microcrystalline samples.*

(b) Amorphous and microcrystalline samples supplied by MV-Systems

We studied the transport properties of three samples supplied by MV-Systems, Inc, Golden, CO, one microcrystalline silicon film (MVS723) and two amorphous silicon films, MVS722 and MVS823. The respective preparation parameters have not been disclosed by MVSystems at this time. Figures 30 - 32 show the respective decay curves for all three samples, whereby the a-Si:H – films are investigated the "classical" way as described earlier.

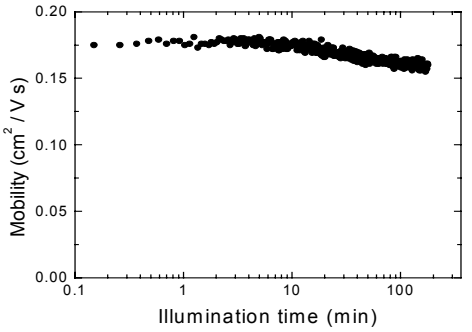

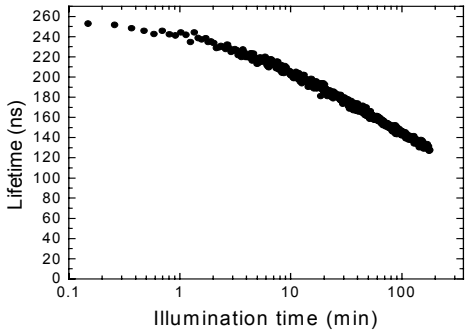

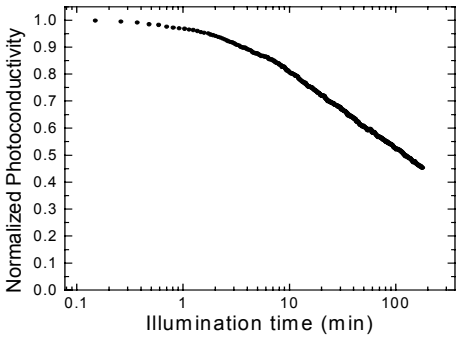

Figure 30.
MVS722 (a-Si:H) Results for the mobility, lifetime, and photoconductivity during light-soaking.

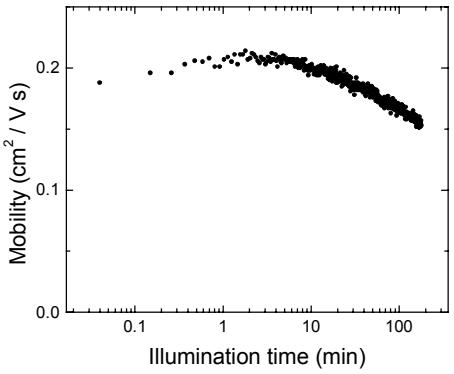

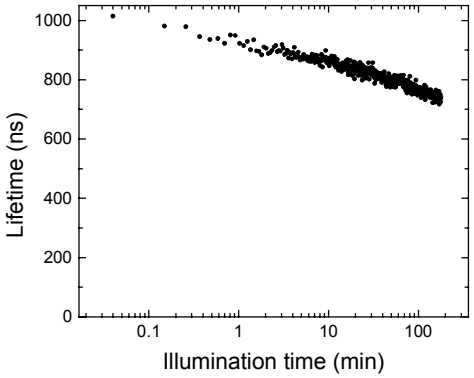

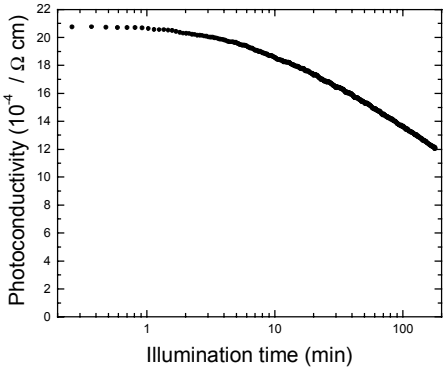

Figure 31.
MVS823 (a-Si:H) Results for the mobility, lifetime, and photoconductivity during light-soaking.

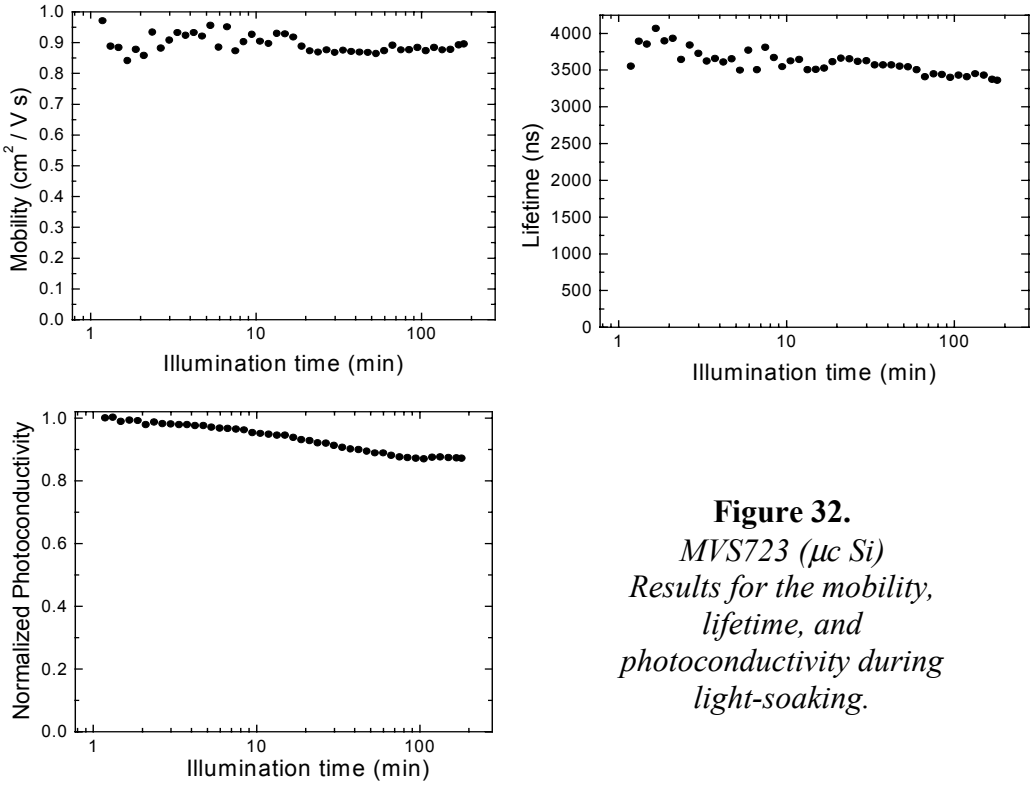

Figure 32.
MVS723 (μc Si) Results for the mobility, lifetime, and photoconductivity during light-soaking.

The range and depth of the long range potential fluctuations (LRPF) of these samples were determined by the electric field dependence of the mobility and are shown in Table 5.

Table 5. LRPF Range and Depth for the MVS – samples (the thickness of the intrinsic layers were about 5000Å).

Sample ID	***Annealed State***		***Light-soaked Sate***	
	Range (nm)	**Depth (eV)**	**Range (nm)**	**Depth (eV)**
MVS722 (a-Si)	52.9	0.125	51.6	0.13
MVS823 (a-Si)	51.8	0.11	53.54	0.13
MVS723 (μc Si)	400	0.08	400	0.082

3. **Improvement of Instrumentation**

Lately, several groups have taken steps into development and investigation of silicon films in the microcrystalline or μc-/a-Si:H mixed state. These films typically show relatively high dark currents at room temperature, which in turn limited the maximum electric BIAS we could apply to rather low values. Accordingly, the accuracy of the photomixing lifetime and mobility determinations suffered from both low electrical fields, i.e. low photomixing signals, and, more seriously, a heating of the sample during measurements which led to an increase of the current of one order of magnitude over the actual photocurrent.

In order to meet the requirements of high accuracy and stable sample temperature, we modified our Photoconductive Frequency Mixing setup and are now able to apply BIAS pulses of arbitrary width and frequency. The dc-current is now monitored sampling the voltage over a 1kΩ resistor by a PC-DAQ board. The whole setup is controlled using LabVIEW programs.

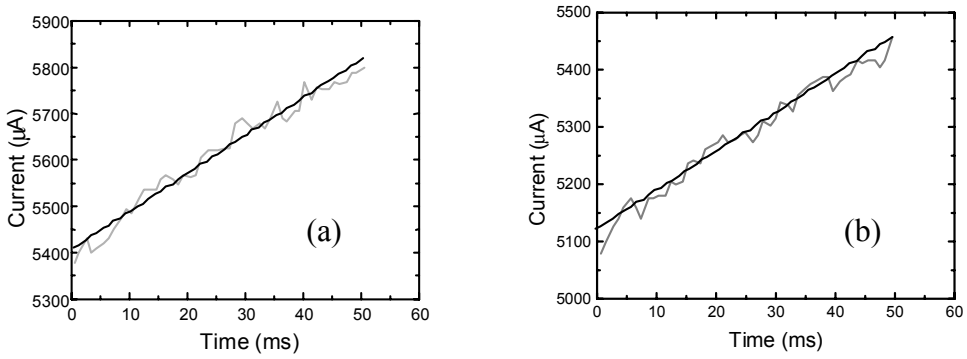

Figure 33. *Current through the μc-Si sample MVS723 (supplied by MVSystems, see previous section) during one 50ms BIAS pulse under illumination (a) and in dark condition (b).*

Figure 33 shows the time dependent dc-current under BIAS application in the dark and illumination case. The sampling rate here is 1000 samples per second (applies for both dc-current and ac-signal), one 50ms - pulse is applied per second whereby one measurement cycle consists of one dark and one light signal acquisition. When the light current is to be measured during a field dependent measurement, the shutter is opened 100ms in advance, which means a total illumination duration of 0.25 seconds per two-second-cycle. In the case of decay measurements, the sample is illuminated 1.75 seconds per cycle. These results are then averaged over at least 100 points for each BIAS point in the field-dependent dc- and ac-curves (see Figure 34).

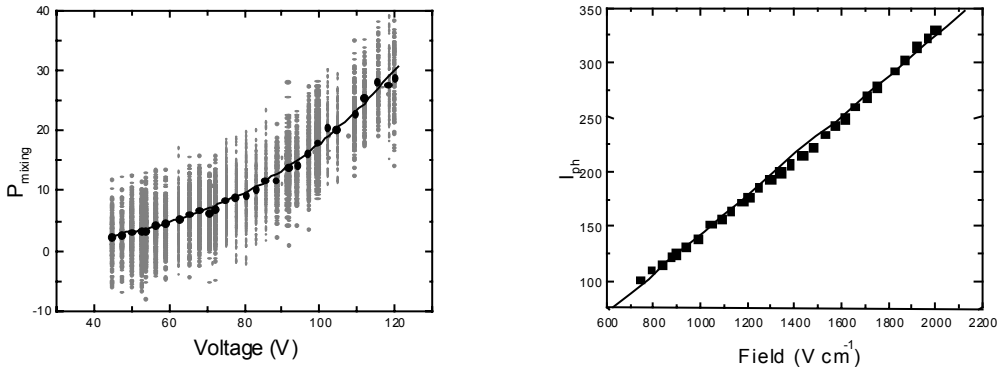

Figure 34. *Photomixing and dc – signal averaging and fitting (solid curves) (sample: MVS723, lightsoaked state).*

As to be seen in the above figure, given enough data points to average, we obtain curves with satisfying accuracy whereas the effective power dissipated within the sample is reduced by a factor of 20 (50ms BIAS vs. 1s per half-cycle). Therefore, electrical fields of much higher magnitude are possible. Also, as shown in figure 33, the slope in the current due to sample heating during one pulse is well defined so that a linear fit yields the currents at room temperature; in addition, they yield a good measure for the temperature stability, i.e. a preferred BIAS-width / frequency ratio.

However, the total illumination duration of about 15 minutes during one field-dependent measurement makes degradation corrections necessary, i.e. data points have to be corrected according to the progress of the transport decay at the time they were taken. For this purpose, decay data that was taken separately is used.

4. Hydrostatic pressure dependence of the charge transport in amorphous silicon

Models to explain the Staebler-Wronski effect in hydrogenated amorphous silicon have been proposed which involve the motion of H atoms. Hydrogen motion in turn may be affected by atomic distances; so it was of interest to study the hydrostatic pressure dependence of the charge transport parameters in amorphous silicon. By employing the photomixing technique, a measurement of the hydrostatic pressure dependence of the mobility and lifetime in the annealed and the light–soaked states could give insight into the dynamics of the Staebler-Wronski effect. Hydrostatic pressure as well as uniaxial stress and substrate misfit stress measurements have been performed over the years; however, at first sight many results seem inconsistent or even contradictory. Many of the measurements employed diamond anvil techniques, which result in uniaxial stress that varies bond angles rather than bond distances; one would expect that the mobility of the hydrogen atoms would be affected by the change in the lattice distance.

For our photomixing measurements we employed a clamped pressure cell with a quartz window. The pressure transmitting fluid was 3M Fluorinert, an electronic fluid with flat optical transmission throughout the visible region and high dielectric strength. The latter is of importance since it is necessary to apply high electric field to the samples in order to measure the electric field dependence of the mobility and so determine the range and the depth of the long-range potential fluctuations. For these initial measurements, an a-Si:H sample produced by the hot-wire technique with 7-9% H was employed.

Figure 35 shows the results of a first pressure dependent photoconductivity measurement of a-Si:H during light soaking. The starting points show that the photocurrent drops with increasing pressure. But also the decay is reduced under higher pressure. The 3 kBar and the 1 kBar curves cross at about 100 minutes which means that after that time the photoconductivity, though starting at a lower value, is still higher after long time irradiation. Figure 36a shows the pressure dependence of the drift mobility as a function of illumination time indicating that at 3 kBar it becomes independent of illumination time. Figure 36b shows the pressure dependence of the lifetime as function of illumination. The lifetime curves though also starting at lower values under pressure show pressure independent slopes.

From this we can conclude that the *generation rate* of recombination centers during light exposition is pressure independent, as well. However, the number of dangling bonds seems to rise under pressure (starting points) which supports the collapsing-void-presumption. The different decay rates of mobility and lifetime under pressure indicate that the rate of generation of charged and neutral scattering defects vary with pressure.

Summarizing our first pressure results one can think of two different ways to describe the pressure dependency of the SW-effect:

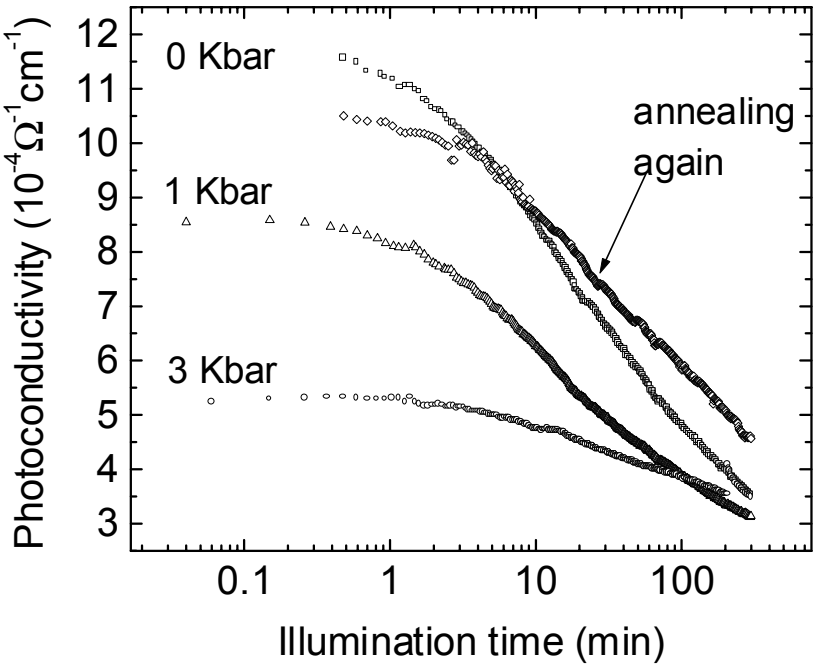

Figure 35: *The Photoconductivity vs. Illumination time for three different pressures. The temporal order of the measurements: 0 kBar ⇒ 1 kBar ⇒ 3 kBar ⇒ 0 kBar ("annealing again") After each turn the sample was reannealed under atmosphere pressure for 1 h at 150 ^{0}C and then put into the pressure cell again.*

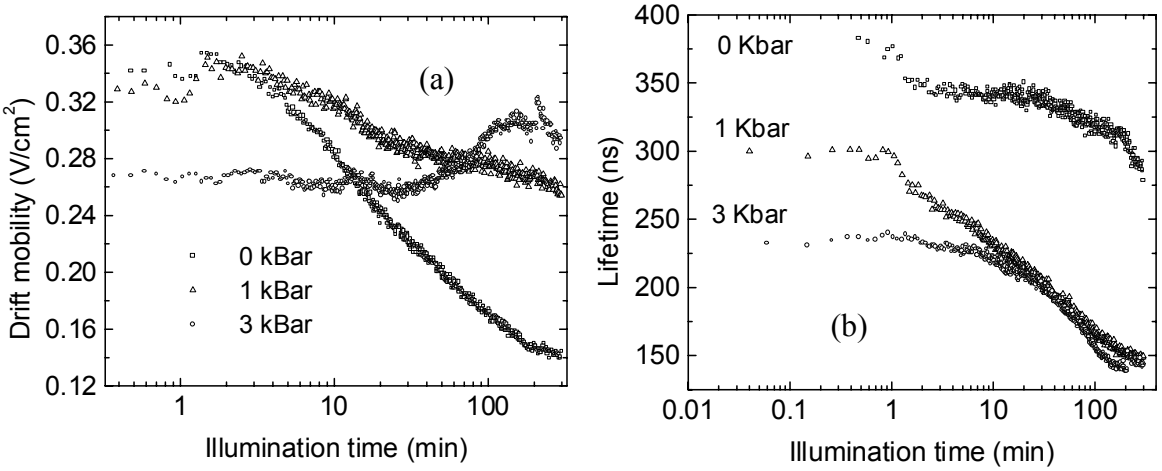

Figure 36. *The drift mobility and lifetime as functions of illumination time under different pressures.*

Under pressure voids can collapse and weak bonds can break resulting in additional dangling bonds reducing both the dark current and photoresponse. This would mean that pressure does more or less the same as light illumination does: it creates local defects.

The pressure dependence of the light soaking experiments may then be regarded as time–shifted. That means, even before illumination there are as many pressure induced defects as though the sample would have been exposed to light as long as it takes to turn down the photoresponse to the value under pressure at the start. These additional dangling bonds result in a decrease in mobility and consequently a decrease in the photoresponse.

It seems possible that pressure application first introduces local defects that can be observed promptly in a change of lifetime and mobility; additionally, pressure related lattice variations change the time dependence of the mobility during illumination which may indicate different generation rates of charged defects. We plan to perform further pressure experiments on samples prepared by different preparation techniques to resolve these questions.

Change of the film thickness after pressure application

Further measurements on the pressure dependence of the transport parameters of amorphous silicon films were performed, with emphasis on possible defects introduced by pressure application. We show both FTIR- and photomixing measurements on amorphous silicon samples.

We measured the change of the IR - spectra of the sample T516 (Qi Wang) first in the annealed state, then after the application of hydrostatic pressure of 3 kBar. After this, we annealed the sample for one hour and repeated the FTIR measurement. From the interference fringes occurring in the spectra it is basically possible to determine the film thickness. The fringes occur as a result of a small refraction index mismatch at the film–substrate-interface ($n=3.0 \leftrightarrow n=3.4$). From the periodicity one can easily determine the respective film thicknesses. Figures 37 and 38 show both the fringes from which the thickness was determined and the results for the respective cases. The initial value of 4.408 μm is in good agreement with the value of 44,100Å given by Qi Wang. After pressurizing the sample the film seems to remain around one hundred nanometers thinner than in the initial state, which would mean a decline of 2.3%. This number seems quite high, though; on the other hand, the apparent thickness change may also be due to a change of the index of refraction. Though reannealing for one hour recovers the sample in part, the thickness remains 40 nm under the initial thickness. However, the results show permanent structural changes introduced by pressure application.

From the actual hydrogen related absorption peaks we could not detect any change in the hydrogen configuration, at least as far as the 2000/2100 – double peak is concerned.

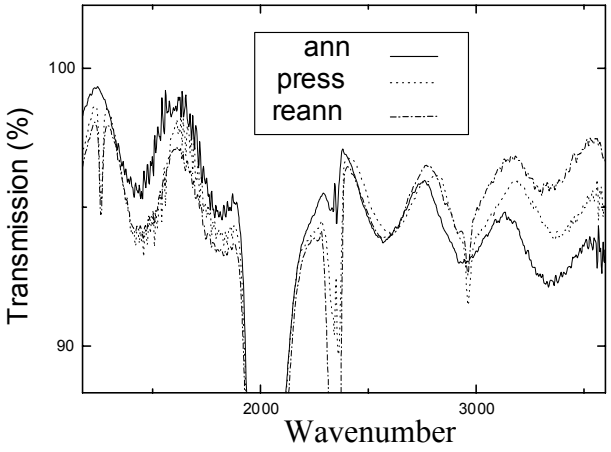

Figure 37. *Infrared transmission of T516 under annealed ("ann"), pressured ("press"), and reannealed ("reann") conditions.*

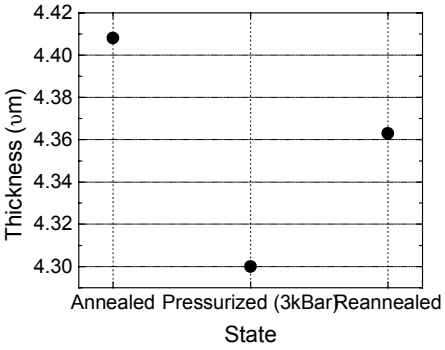

Figure 38.
T516 – film thickness after pressure application.

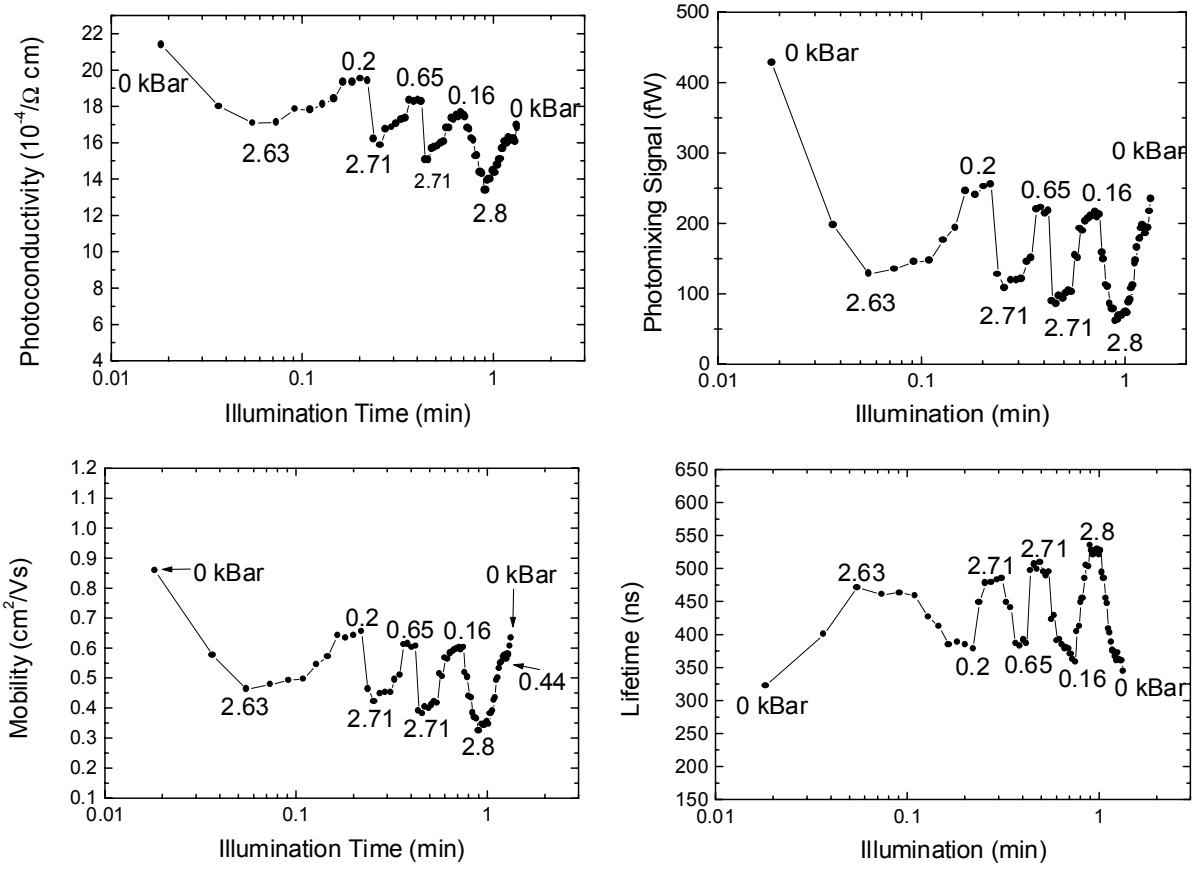

Figure 39. *Pressure-dependent transport parameters. After initial annealing, the sample was pressurized and released again. We performed four cycles in the same way, with the transport parameters monitored in situ. The x-axis position is associated with the over-all illumination period during the measurement.*

Transport vs. Pressure Hysteresis Measurements

Four cycles with a pressure from 0 to 2.8 kBar being applied and released were run during the measurement. The photoconductivity, mobility, and lifetime were measured at each stage. The results are shown in the figure 39. It was found that under a given pressure the photoconductivity and mobility decreased while the lifetime increased. However, when the pressure was released a partial recovery of the photoconductivity and mobility was observed but not to the values obtained at the initial zero pressure. These results indicate that there are two effects of hydrostatic pressure; one an *elastic* effect where the mobility decreases under pressure but is restorable when the pressure is released and an inelastic effect where the mobility is decreased due to the introduction of charge scattering centers.

In order to illucidate the participating effects in amorphous silicon under pressure we also performed a similar measurement on single crystalline silicon with the results shown in figure 40. They show that for single crystals there is only an elastic effect.

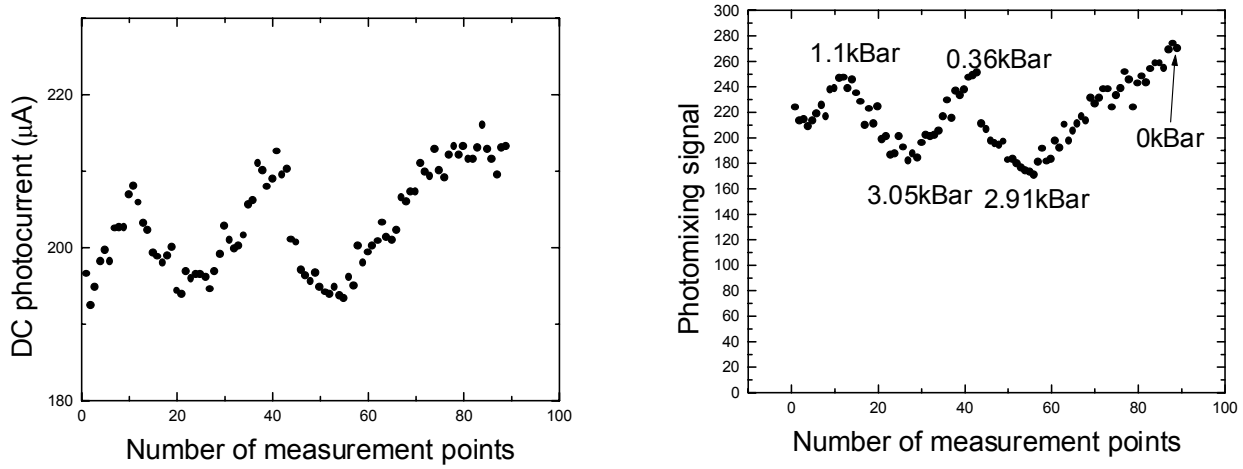

Figure 40. *DC photocurrent and photomixing signal under different pressures in single crystalline silicon. Both decrease with increasing pressure. The curves show only an elastic effect.*

5. Photomixing Measurements on SiGe P-I-N Devices
(Supplied by Xunming Deng, Univerity of Toledo)

The photomixing measurement method has been shown to be a successful tool in determining photomixing lifetime and mobility of charge carriers in amorphous and microcrystalline silicon as well as silicon-germanium and other alloy films which are measured in in-plane direction employing coplanar contacts. Here, one deals with a well defined uniform electric field due to an external voltage, a spacially uniform distribution of charged and neutral defects, and a free charge carrier generation profile perpendicular to the field direction.

In p-i-n structures, in contrast to single films with coplanar ohmic contacts, one usually finds

- a space charge distribution in the intrinsic layer near the p-i and i-n interfaces
- a non-uniform electron-hole generation profile in field direction
- and thus a generally non-uniform electric field distribution across the i-layer

Additionally, the ac behavior of a p-i-n device is determined by the device geometry and the resulting capacitance. On the other hand, due to the high mixing frequency used, the transient behavior does not play an important role.

The BIAS dependent photomixing power that one detects for different devices under different illumination conditions is thus necessarily affected by many more parameters than it is in the case of single layer films. Even worse, some of the parameters, particularly the electric field distribution, depends on both the deployed materials and the interfaces in a complicated way that is still not very well understood. Therefore, instead of incorporating many unknown parameters into the photomixing model, it seems more advisable to restrict measurements and data analysis to certain regimes where at least analytical models based on simplified assumptions may be valid.

The most important analytical approach is probably the uniform-field model by Crandall [17], whose main assumptions are: uniform field, negligible diffusion in the intrinsic layer, and the use of the Shockley-Read-Hall model for recombination for a two state recombination center. Later, Hubin and Shah [18] presented a variation of Crandall's model introducing three-states recombination centers. The majority of publications, however, present numerical approaches which might yield more realistic results but have the drawback of making it hard to draw immediate physical conclusions. In a recent publication by Asensi et al [19], analytical expressions for the recombination current and the short-circuit resistance are deduced from results of numerical simulations.

Dangling bonds within the intrinsic layer near the interfaces are thought to be usually charged due to the relative shift of the Fermi level to the defect states. Dangling bonds in a charged state, in turn, have a much higher cross section as recombination centers so that

a main part of the total recombination processes in the i-layer - which represent the main limitation of the p-i-n-cell efficiency - is assumed to take place near the interfaces. Moreover, these dangling bond states near the interfaces build up space charge regions which lead to higher electric field strengths near the interfaces and accordingly lower fields in the center. In fact, the thickness of the i-layer is usually kept as thin as possible, so that even with a certain space charge present, the field near the center is sufficiently strong to deplete the generated charge carriers.
However, according to Asensi et al., a uniform-field approximation is possible in the special case of high illumination intensity ($I_{short\text{-}circuit}$ > 10mA cm^{-2}) and short circuit or back-biasing condition, i.e. when the charged defect states near the p-i and i-n interfaces are neutralized and no charge injection into the intrinsic layer takes place. In this situation, with space charge regions depleted through the strong illumination, also secondary quantities affecting the photomixing power like the device capacitance should not change dramatically with different bias voltages in reverse direction.
The photomixing technique, due to the high beating frequency, merely yields a picture of shallow trap states near the conduction band and is insensitive to deep level defects. Therefore, only for the above mentioned conditions it seems possible to obtain information about the transport properties of the intrinsic layer without the need to deconvolute a complex amount of parameters most of which are not even known. On the other hand, this might enable us to keep track of a certain material-related aspect, i.e. the charge carrier mobility, which is otherwise somewhat lost once single films are deposited within a multilayer structure.

Figures 41 shows the square root of the photomixing power under back-biasing.

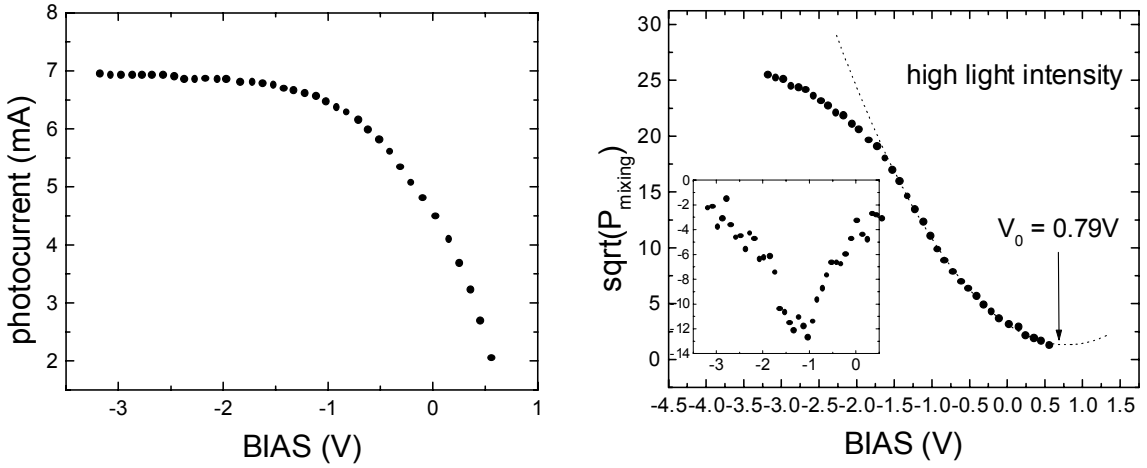

Figure 41. *DC photocurrent and the square root of the photomixing power (inset: derivative of sqrt(P_{mix})).*

While the dc photocurrent shows expected saturation behavior when the p-i-n device is reverse-biased, in the case of the ac current (as represented by the square root of the mixing power) we find (at least) two distinct regimes, a low-field and a high-field regime.

In the high-field regime, we find an increase with a saturation tendency at sufficiently high fields. The mobility of electrons in a p-i-n structure when approaching high fields has been described in terms of field-assisted thermal release of electrons from traps within the multiple trapping model [20].
However, for biases below the point of inflection, the shape of the curve rather resembles the field-dependent mobility which is also observed in thin film samples with coplanar contacts. The dotted curve which is fit into the lower-field part of the photomixing current curve points out where the photomixing signal deviates from it's initial shape. According to this fit, the photomixing signal would become zero at about +0.8V, which would mean that at this point the built-in field zero-crosses.

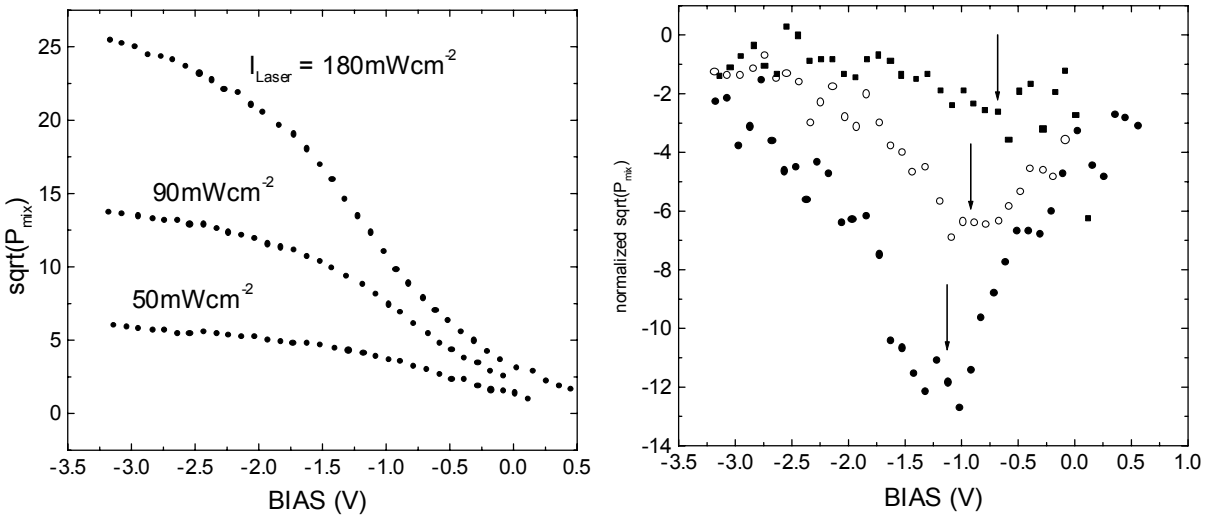

Figure 42. *Light intensity dependent photomixing current. Right hand-side: The derivatives show a shift of the point of inflection to higher biases at higher light intensities.*

However, this fitting only works for high illumination levels. For lower light intensities we observe a shift towards higher electric fields (figure 42). It is noteworthy, however, that even for (very) high illumination levels a uniform field within the intrinsic layer is at best a good approximation. For lower levels, this simplified model is certainly not feasible. Absolute values for the mobility across the intrinsic layer seem therefore – in contrast to single films – not very meaningful. However, investigating the evolution of the bias-dependent photomixing curves under light-soaking provide a separation of effects due to geometric or initial material properties from those due to light-induced defects as the following figures show.

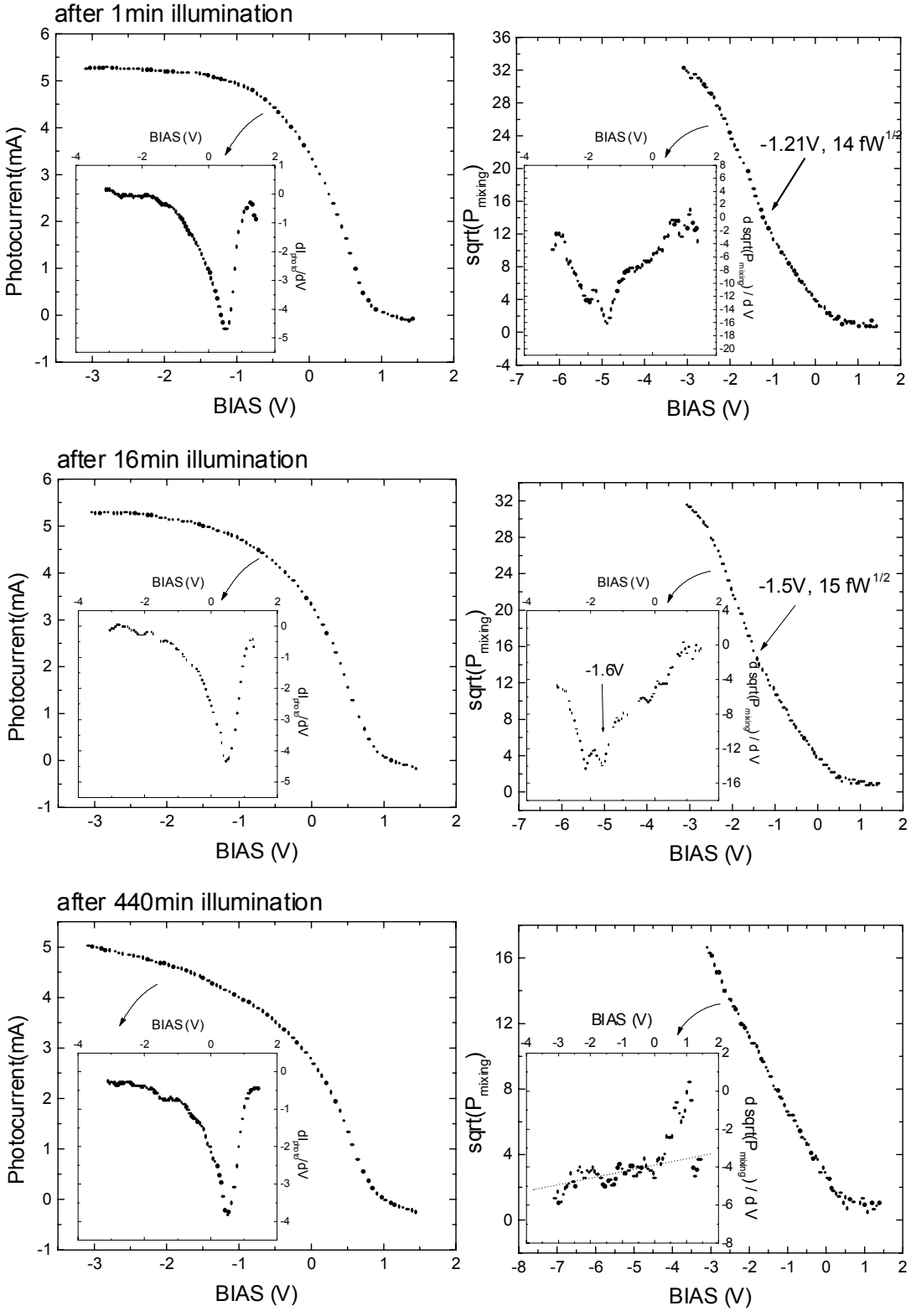

Figure 43. *dc and mixing currents after different illumination times (Sample Toledo-GD112).*

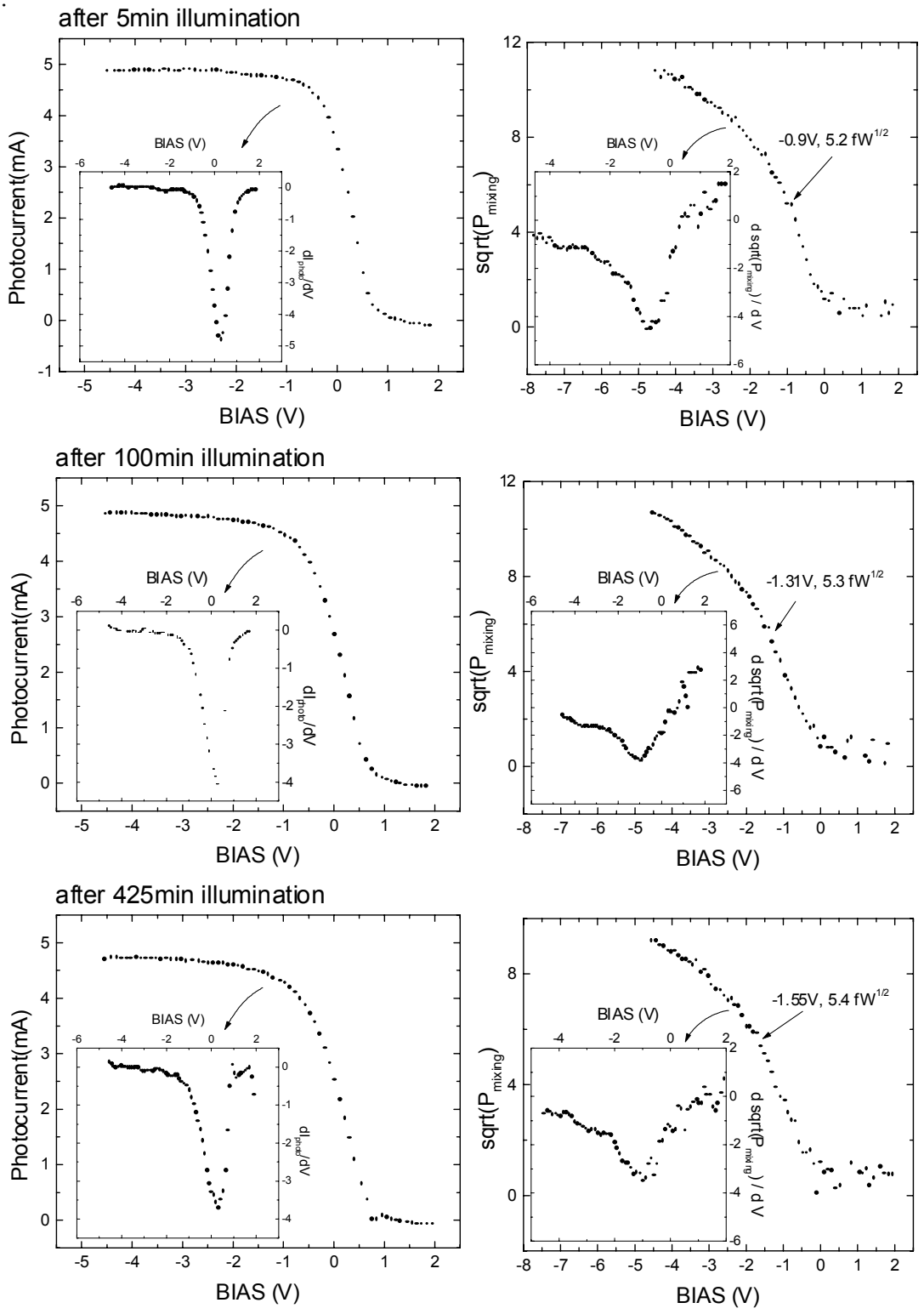

Figure 44. *dc and mixing currents after different illumination times (Sample Toledo-GD111).*

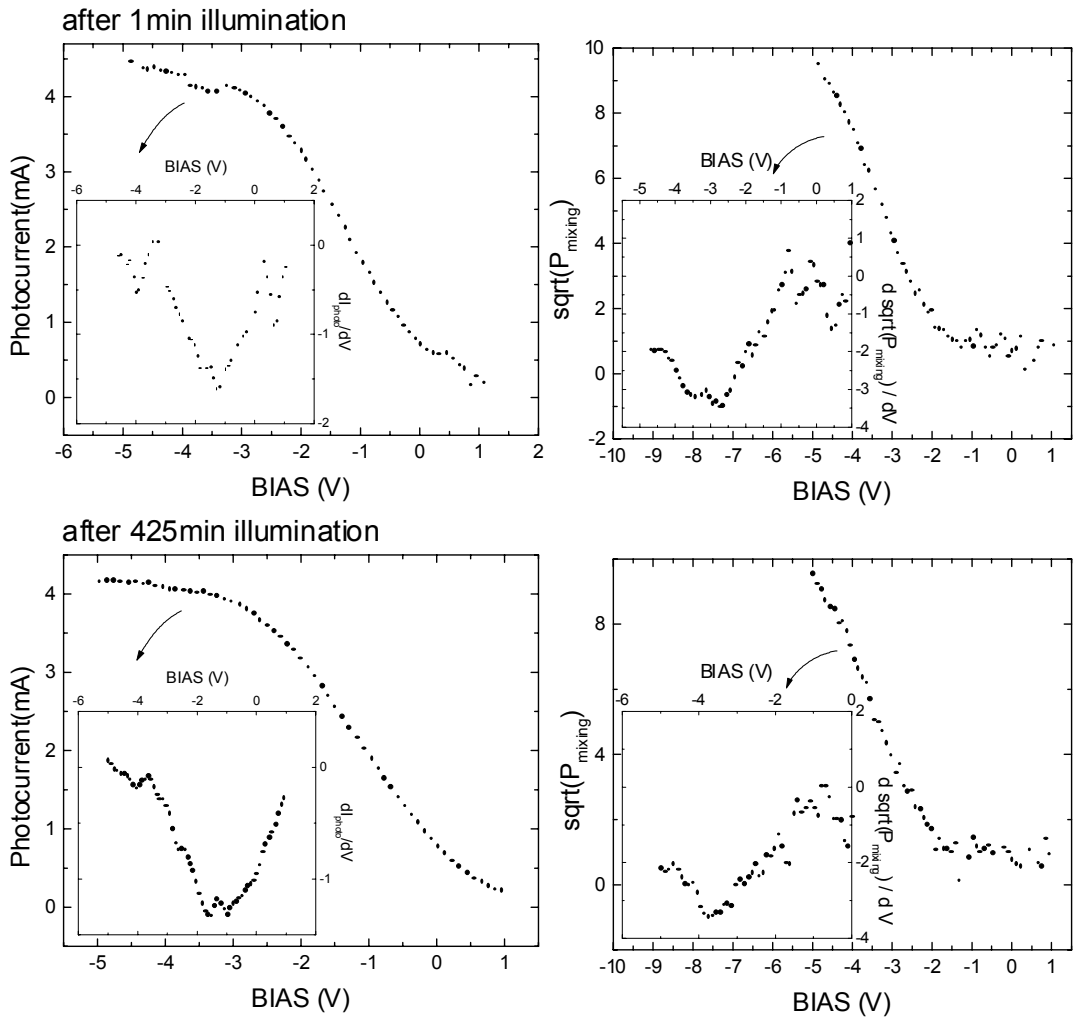

Figure 45. *Sample Toledo-GD110.*

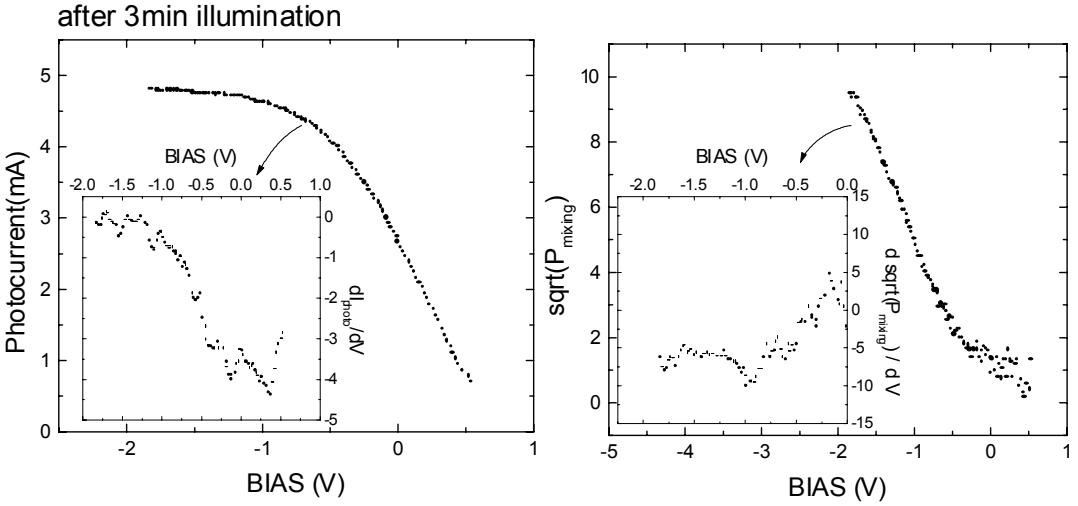

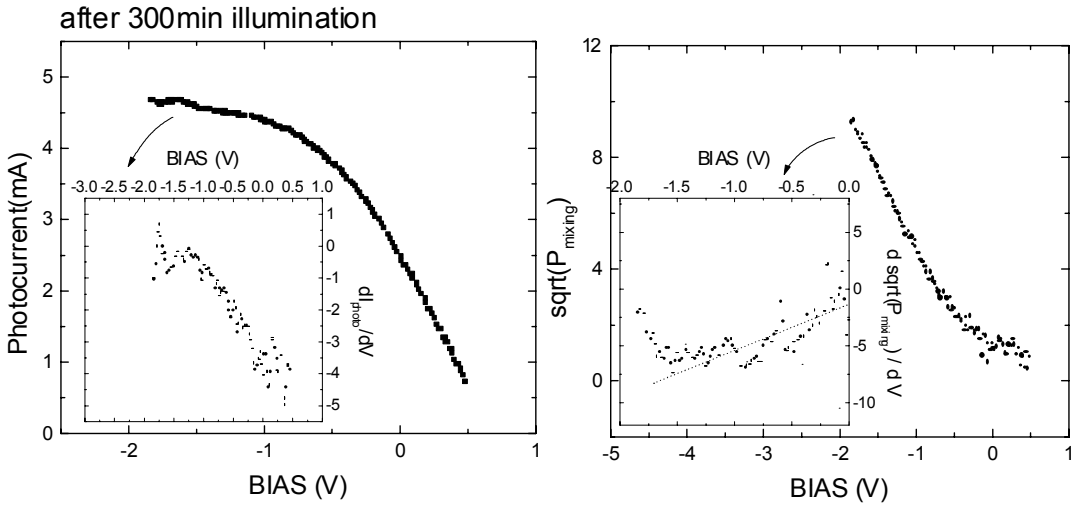

Figure 46. *dc and mixing currents after different illumination times (Sample Toledo-GD109).*

Figures 43-46 show data obtained from light-soaking measurements on p-i-n-samples supplied by the Toledo group. The insets contain the neighbor-averaged derivatives of their parent curves in order to facilitate the observation of the change of the curve shape during light-soaking. A summary of the respective I-V data can be found in Table 5.

Table 6. *I-V data for a-SiGe solar cells with different i-layers (~2000Å)*

Sample	V_{oc} **(V)**	J_{ph} from QE (mA/cm^2)	FF	P_{max} (mW/cm^2)
GD109 Standard	0.681	19.3	0.530	6.97
GD110 +15% Ge	0.634	21.3	0.473	6.39
GD111 -15% Ge	0.714	20.0	0.527	7.53
GD112 2.5x H dilution	0.813	18.2	0.486	7.19

Sample GD112 shows both the highest mixing signals and the largest decay under light-soaking. However, according to data from Toledo (table 5) this sample's filling factor is the second worst of all samples. It is obvious that the dc p-i-n cell performance and the photomixing signal, even though associated with the charge carrier mobility, do not directly scale. This was not to be expected, though. It is clear that the actual device impedance has a great impact on the photomixing signal power. A comparison of the photomixing curves for two different *spots* on the same sample (GD112) as shown in figure 47 stresses this point.

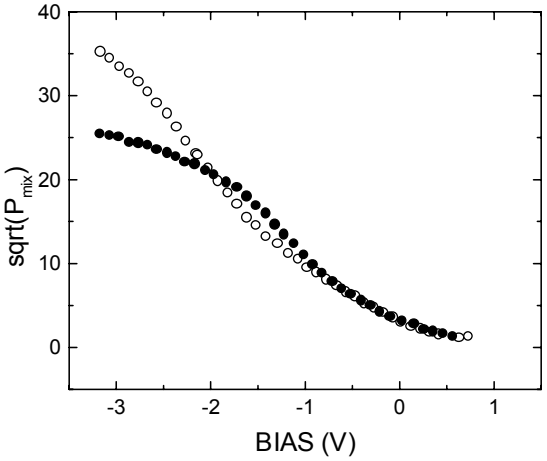

Figure 47. *BIAS-dependent ac – photocurrent for two different spots*

At one spot ('spot' means one separate p-i-n-structure among others on the same stainless steel substrate) the curve reaches saturation behavior earlier but at lower mixing signals than it does at some other spot. A steeper curve at lower fields and consequently earlier onset of saturation would mean higher mobility while the variation in mixing power is rather due to the differences in the sample impedance which is apparently quite sensitive to fabrication variations. In contrast to this effect the changes during light soaking (figure 43), i.e. with parameters other than the defect density kept constant, suggest that the charged defect related field-dependent mobility regime extends to higher electric fields across the i-layer at the saturation regime's expense. After seven hours of light exposure, the saturation regime vanishes completely which means that the applied bias has become insufficient in order for the degraded sample to enter this region. It is also noteworthy that the point of inflection, as marked within the first two viewgraphs of figure 43, seems to more or less remain at the same height while wandering towards higher biases. After 425 minutes, the photomixing current just reaches the 16 $fW^{1/2}$ level from which the saturation regime evolved in the annealed state. Note also that the dc-current curve seems less affected than the ac-curve. In all samples except for GD110, which turns out be the most stable one, we find the slope of the ac-curve within the lower-field regime to decrease with illumination time. Unfortunately, in most cases we had to limit the maximum reverse bias in order to protect the samples from avalanching. On the other hand, former measurements on a-Si samples showed saturation much more clearly - probably because the electron mobility is generally higher in a-Si than in a-SiGe.

In order to obtain at least approximate values for the electron mobility in p-i-n-structures the photoconductive frequency mixing model has to be adapted appropriately. In particular, the capacitance and geometry contributions will have to be treated in such a way that the ac-signal dependent transport expressions become independent of those. Therefore, accompanying ac-measurements are needed. In a next step, the photomixing transport equations have to be applied and tested against results from further measurements on a series of n-i-p-solar cells supplied by the Toledo group.

We also plan a series of experiments on samples in coplanar configuration and p-i-n-devices that are prepared under the same growth condition.

As far as the experiment is concerned, a higher accuracy, particularly of the ac-current curve derivative, is desirable. One possible way to obtain more accurate results is a more direct measurement of the derivative of the mixing power. Initial experiments employing low-frequency bias sweep and log-in amplification techniques are promising. However, there is always a certain trade-off between measurement accuracy and the undesirable light-soaking effect during the acquisition of a photomixing signal curve.

REFERENCES

1. E.R.Geissinger, R. Braunstein, S.Dong, and R. Martin, J. Appl .Physics **69**, 1469 (1991).

2. Y. Tang, R. Braunstein, and B. von Roedern, Appl. Phys. Lett. **63** 2393 (1992).

3. Y.Tang, R. Braunstein, B. von Roedern, F.R. Shapiro. Mater. Res. Soc Symposium Proc **297,** 407 (1993).

4. Y. Tang and R. Braunstein, Appl. Phys. Lett. **66** 721 (1995).

5. Y. Tang and R. Braunstein, J. Appl. Phys.**79** 850 (1996).

6. Y. Tang, S. Dong, R. Braunstein, and B. von Roedern, Appl. Phys. Lett. **68** 640, (1996).

7. Meier, P. Torres, R. Platz, S.Dubail, U. Kroll, J.A. Anna Selvan, N. Pellton Vaucher, Ch. Hof, D. Fischer, H. Keppner, A. Sha, K. D. Lifert, P. Giannulés, J. Koehler, MRS Symp. Proc. **420** (1996).

8. D.V. Tsu, B.S.Cho, S.R.Ovshinsky, S. Guha and J. Yang, Appl Phys. Lett. **71**, 1317 (1997).

9. H. Wiesmann, A. K. Ghosh, T. McMahon, and M. Strongin, J. Appl. Phys. **50**, 3752 (1979).

10. H. Matsumera. Jpn. J Appl. Phys., Part 2, **25**, L949 (1986).

11. J. Cifre, J.Bertomeu, J. Puigdollers, M.C. Polo, J. Andreu, and A. Lioret, Appl. Phys. A: Solids Surf. **59**, 645 (1994).

12. A. R. Middya, J. Guillet, J. Perrin, A. Lioret, and J.E.Boirree in *Proccedings of the 13th European Photovoltaic Solar Energy Conference, Nice* 1995 edited by W. Freiesleben, W. Palz, H.A. Ossenbrink and P. Helm (H.S. Stephens & Associates, Bedford, U. K., 1995). p. 3.

13. M. Heintze, R..Zedlitz, H.N.Wanka, and M. B.Schubert, J. Appl. Phys. **79**, 2699 (1996).

14. F. Diehl, W. Herbst, B. Schröder, H. Oechsner, MRS Symp. Proc. **467** (1997), 451.

15. R. Brüggemann, C Main Phys. Rev. D **57,** R15080 (1998).

16. A. A. Langford, M. L. Fleet, B. P. Nelson, W. A. Lanford, and N. Maley, Phys. Rev. B **45**, 13367 (1992)

17. R.S. Crandall, J. Appl. Phys. **54,** 7176 (1983).

18. J. Hubin and A. V. Shah, Philos. Mag. B **72,** 589 (1995).

19. J. M. Alensi, J. Merten, C. Voz, and J. Andreu, J. Appl. Phys. **85,** 2939 (1999).

20. G. Juska, K. Arlauskas, J. Kocka, M. Hoheisel, and P. Chabloz, Phys. Rev. Let **75**, No. 16, 2984 (1995)

REPORT DOCUMENTATION PAGE

Form Approved
OMB NO. 0704-0188

1. AGENCY USE ONLY (Leave blank)	2. REPORT DATE	3. REPORT TYPE AND DATES COVERED
	February 2000	Annual Subcontract Report, 20 April 1998–19 April 1999

4. TITLE AND SUBTITLE
Photocharge Transport and Recombination Measurements in Amorphous Silicon Films and Solar Cells by Photoconductive Frequency Mixing; Annual Subcontract Report, 20 April 1998–19 April 1999

5. FUNDING NUMBERS
C: XAK-8-17619-24
TA: PV005001

6. AUTHOR(S)
R. Braunstein, A. Kattwinkel, J. Liebe, and G. Sun

7. PERFORMING ORGANIZATION NAME(S) AND ADDRESS(ES)
Department of Physics and Astronomy
University of California
Los Angeles, CA 90095

8. PERFORMING ORGANIZATION REPORT NUMBER

9. SPONSORING/MONITORING AGENCY NAME(S) AND ADDRESS(ES)
National Renewable Energy Laboratory
1617 Cole Blvd.
Golden, CO 80401-3393

10. SPONSORING/MONITORING AGENCY REPORT NUMBER
NREL/SR-520-27931

11. SUPPLEMENTARY NOTES
NREL Technical Monitor: B. von Roedern

12a. DISTRIBUTION/AVAILABILITY STATEMENT
National Technical Information Service
U.S. Department of Commerce
5285 Port Royal Road
Springfield, VA 22161

12b. DISTRIBUTION CODE

13. ABSTRACT *(Maximum 200 words)*
In the present phase of the program, the transport parameters of a number of amorphous semiconductors prepared by a number of techniques were determined by the photoconductive frequency mixing technique. This technique enabled us to determine the drift mobility, μ_d, and the photomixing lifetime, τ. The technique is based on the idea of heterodyne detection for photoconductors. When two similarly polarized monochromatic optical beams of slightly different frequencies are incident upon a photoconductor, the generation rate of electron-hole pairs will produce a photocurrent, when a dc-bias is applied, which will contain components resulting from the square of the sum of the individual incident fields. Consequently, a photocurrent will be produced, which will consist of a direct current and a microwave current corresponding to the beat frequency. These two currents allow a separate determination of the drift mobility and the photomixing lifetime of the photogenerated carriers. In the present work, the longitudinal modes of a He-Ne laser were employed to generate a beat frequency of 252 MHz; all the measurements were performed at this frequency for the data indicated in the accompanying figures. The following topics were explored:

- Measurements of the charge transport parameters of homogeneous a-SiGe:H alloys produced by NREL employing the hot-wire technique.
- The change in the charge transport parameters in the transition from hydrogenated amorphous silicon to microcrystalline silicon for material produced by NREL and MVSystems.
- The improvement in instrumentation of the photomixing measurements.
- Measurements of the hydrostatic dependency of the transport parameters of amorphous silicon.
- Preliminary photomixing measurements on p-i-n devices.

14. SUBJECT TERMS
photovoltaics ; photocharge transport ; recombination measurements ; amorphous silicon films ; solar cells ; photoconductive frequency mixing ; hydrogenated amorphous silicon ; microcrystalline silicon ; heterodyne detection ; beat frequency

15. NUMBER OF PAGES

16. PRICE CODE

17. SECURITY CLASSIFICATION OF REPORT	18. SECURITY CLASSIFICATION OF THIS PAGE	19. SECURITY CLASSIFICATION OF ABSTRACT	20. LIMITATION OF ABSTRACT
Unclassified	Unclassified	Unclassified	UL